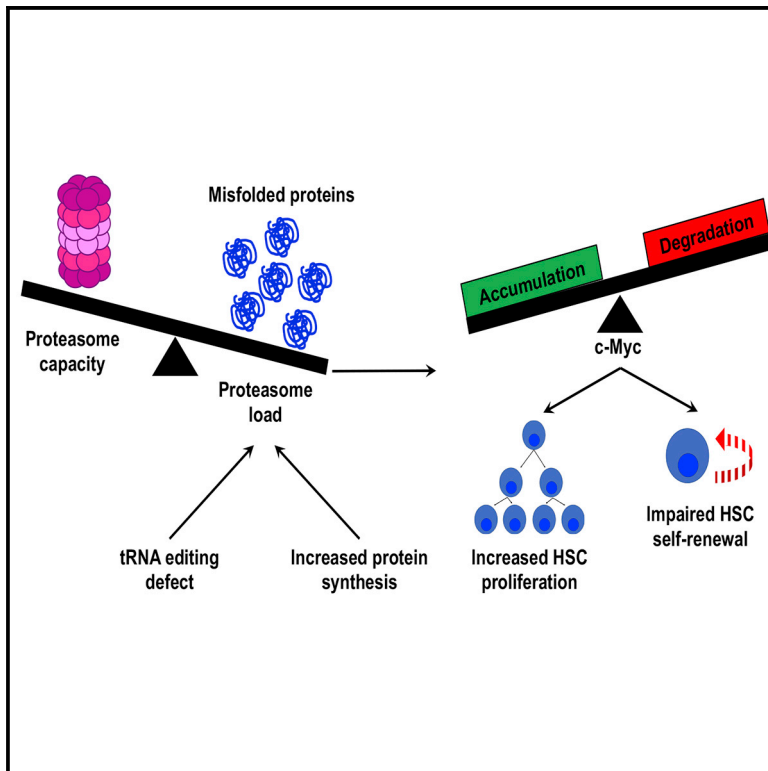


Modest Declines in Proteome Quality Impair Hematopoietic Stem Cell Self-Renewal

Graphical Abstract



Authors

Lorena Hidalgo San Jose,
Mary Jean Sunshine,
Christopher H. Dillingham, ...,
Yuning Hong, Danny M. Hatters,
Robert A.J. Signer

Correspondence

rsigner@ucsd.edu

In Brief

Stem cells in multiple tissues depend on low protein synthesis to promote regeneration. Hidalgo San Jose et al. demonstrate that low protein synthesis promotes hematopoietic stem cell function by restricting the biogenesis of misfolded proteins. Misfolded proteins impair stem cell quiescence and self-renewal by overwhelming the proteasome and disrupting proteostasis.

Highlights

- HSCs have fewer misfolded and unfolded proteins than restricted myeloid progenitors *in vivo*
- HSCs depend on low protein synthesis to maintain their elevated proteome quality
- tRNA editing defect impairs HSC self-renewal by increasing genesis of misfolded proteins
- Misfolded proteins overwhelm proteasome in HSCs, leading to c-Myc accumulation



Modest Declines in Proteome Quality Impair Hematopoietic Stem Cell Self-Renewal

Lorena Hidalgo San Jose,^{1,4} Mary Jean Sunshine,^{1,4} Christopher H. Dillingham,^{1,4} Bernadette A. Chua,^{1,4} Miriama Kruta,¹ Yuning Hong,² Danny M. Hatters,³ and Robert A.J. Signer^{1,5,*}

¹Division of Regenerative Medicine, Department of Medicine, Moores Cancer Center, University of California San Diego, La Jolla, CA 92093, USA

²Department of Chemistry and Physics, La Trobe Institute for Molecular Science, La Trobe University, Melbourne, VIC 3083, Australia

³Department of Biochemistry and Molecular Biology, Bio21 Molecular Science and Biotechnology Institute, The University of Melbourne, Parkville, VIC 3010, Australia

⁴These authors contributed equally

⁵Lead Contact

*Correspondence: rsigner@ucsd.edu

<https://doi.org/10.1016/j.celrep.2019.12.003>

SUMMARY

Low protein synthesis is a feature of somatic stem cells that promotes regeneration in multiple tissues. Modest increases in protein synthesis impair stem cell function, but the mechanisms by which this occurs are largely unknown. We determine that low protein synthesis within hematopoietic stem cells (HSCs) is associated with elevated proteome quality *in vivo*. HSCs contain less misfolded and unfolded proteins than myeloid progenitors. Increases in protein synthesis cause HSCs to accumulate misfolded and unfolded proteins. To test how proteome quality affects HSCs, we examine *Aars*^{sti/sti} mice that harbor a tRNA editing defect that increases amino acid misincorporation. *Aars*^{sti/sti} mice exhibit reduced HSC numbers, increased proliferation, and diminished serial reconstituting activity. Misfolded proteins overwhelm the proteasome within *Aars*^{sti/sti} HSCs, which is associated with increased c-Myc abundance. Deletion of one *Myc* allele partially rescues serial reconstitution defects in *Aars*^{sti/sti} HSCs. Thus, HSCs are dependent on low protein synthesis to maintain proteostasis, which promotes their self-renewal.

INTRODUCTION

Adult hematopoietic stem cells (HSCs) synthesize less protein per hour than most other hematopoietic progenitors. This does not simply reflect HSC quiescence because dividing HSCs also have lower rates of protein synthesis than dividing restricted progenitors (Signer et al., 2014). Low protein synthesis is necessary for HSC maintenance, as genetic changes that modestly increase protein synthesis impair HSC function (Goncalves et al., 2016; Signer et al., 2014, 2016). Somatic stem cells in multiple other adult tissues also have relatively low rates of protein synthesis, and this is often necessary for stem cell maintenance (Blanco et al., 2016; Llorens-Bobadilla et al., 2015; Sanchez et al., 2016; Zismanov et al., 2016). This raises a fundamental

question of why low protein synthesis is necessary for stem cell maintenance and tissue regeneration.

Translation is the most error-prone step in gene expression. Translational errors can lead to protein misfolding and the formation of toxic aggregates. High rates of protein synthesis can increase amino acid misincorporation (Drummond and Wilke, 2009). Reducing translation decreases the synthesis of defective translational products and promotes the clearance of misfolded proteins (Sherman and Qian, 2013). Based on these observations, we hypothesized that low protein synthesis could promote HSC maintenance and function by enhancing proteome quality, which we define as limiting the abundance of mistranslated, unfolded, and/or misfolded proteins. In this study, we set out to examine the effect of protein synthesis rates on proteome quality within HSCs *in vivo* and to test the consequences of reducing protein quality on HSC function.

RESULTS

HSCs Contain Less Ubiquitylated and Unfolded Protein Than Myeloid Progenitors

To assess proteome quality within hematopoietic stem and progenitor cells, we measured the abundance of ubiquitylated protein by western blot. Ubiquitylated protein includes an abundance of mistranslated or damaged proteins that misfold and are targeted for degradation (Duttler et al., 2013; Kim et al., 2011; Wang et al., 2013). As a consequence, ubiquitylated protein is widely used to assess the abundance of misfolded and unfolded proteins (Kim et al., 2011; Lee et al., 2006; Schubert et al., 2000). To obtain enough cells for western blot analyses, we typically pooled CD150⁺CD48⁻ Lineage⁻Sca-1⁺c-kit⁺ (CD150⁺CD48⁻LSK) HSCs (Kiel et al., 2005) and CD150⁻CD48⁻LSK multipotent progenitors (MPPs) (Oguro et al., 2013). HSCs and this population of MPPs (which are sometimes referred to as short-term HSCs) are very similar in terms of their gene expression profile (Signer et al., 2016), cell cycle status (Oguro et al., 2013), protein synthesis rate (Signer et al., 2014), and metabolism (Agathocleous et al., 2017). CD48⁻LSK HSCs/MPPs contained considerably less ubiquitylated protein and less LysK48-linkage specific polyubiquitylated protein (which preferentially targets substrates for degradation) than equal



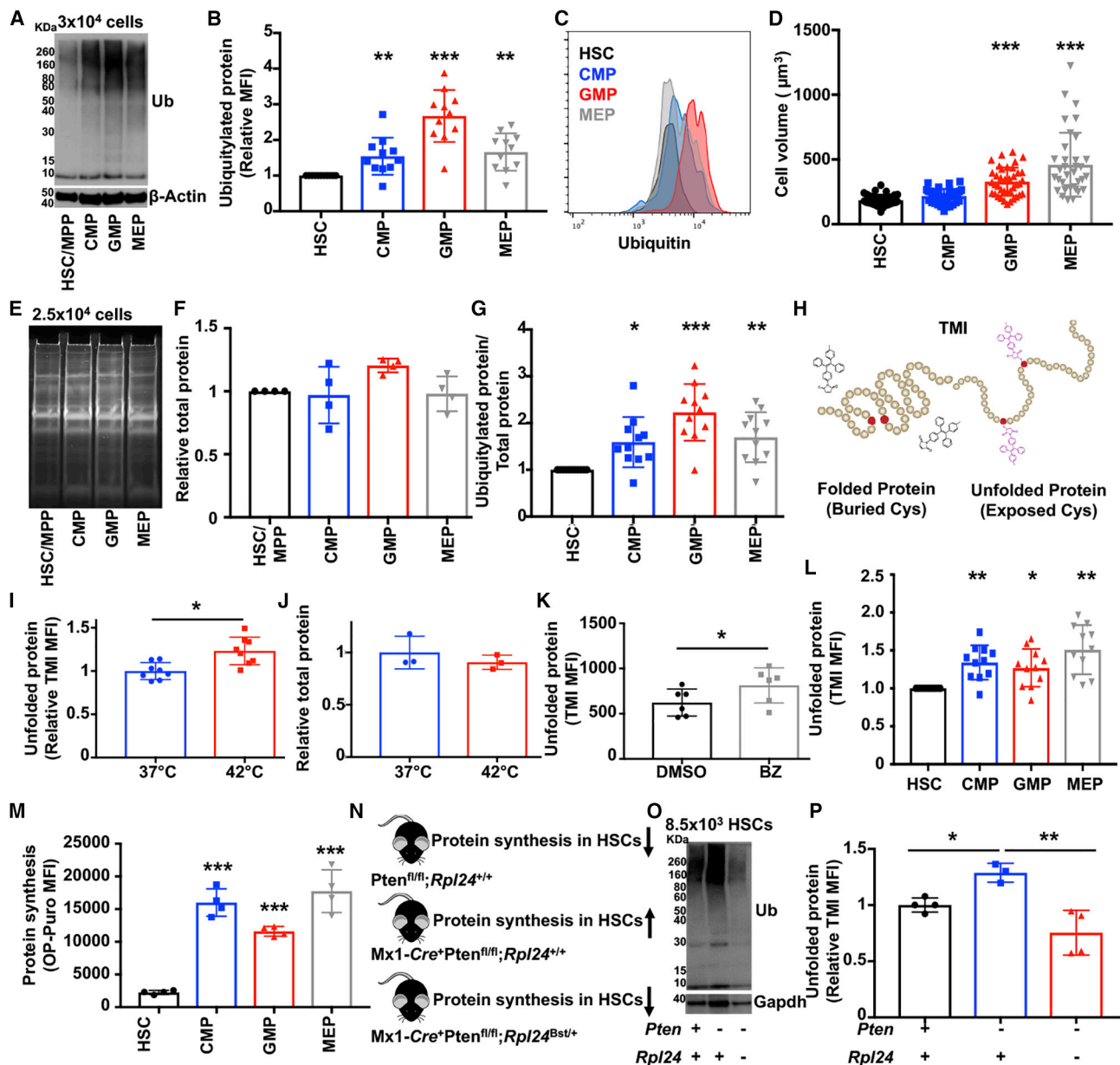


Figure 1. HSCs Depend upon Low Protein Synthesis to Maintain Proteome Quality

(A) Western blot examining ubiquitylated protein in 3×10^4 HSCs/MPPs, CMPs, GMPs, and MEPs (one of >5 blots).
 (B) Flow cytometry analysis showing ubiquitylated protein content relative to HSCs (n = 11 mice).
 (C) Representative histograms of ubiquitylated protein content in HSCs, CMPs, GMPs, and MEPs.
 (D) Cell volume of HSCs, CMPs, GMPs, and MEPs (n \geq 34 cells/population).
 (E) Representative gel showing total protein content following SYPRO Ruby staining in HSCs/MPPs, CMPs, GMPs, and MEPs (one of 4 blots).
 (F) Total protein content relative to HSCs (n = 4 experiments).
 (G) Ubiquitylated protein relative to total protein content in HSCs, CMPs, GMPs, and MEPs (from B and E).
 (H) Diagram showing that TMI fluoresces when it binds to free cysteine thiols in unfolded proteins.
 (I) Relative TMI fluorescence in bone marrow cells after a 4-h incubation at 37°C or 42°C (n = 8 mice).
 (J) Total protein content in bone marrow cells after a 4-h incubation at 37°C or 42°C (n = 3 mice).
 (K) TMI fluorescence in bone marrow cells from mice treated 18 h earlier with bortezomib (BZ) or vehicle (DMSO) (n = 6 mice/treatment).
 (L) Relative TMI fluorescence in HSCs and progenitors (n = 11 mice).
 (M) OP-Puro incorporation by HSCs, CMPs, GMPs, and MEPs *in vivo* (n = 4 mice).
 (N) Diagram representing effects on HSC protein synthesis in wild-type (*Pten^{fl/fl};Rpl24^{+/+}*), *Pten*-deficient (*Mx1-Cre⁺Pten^{fl/fl};Rpl24^{+/+}*), and *Mx1-Cre⁺Pten^{fl/fl};Rpl24^{Bst/+}* mice.

(legend continued on next page)

numbers of common myeloid progenitors (CMPs), granulocyte macrophage progenitors (GMPs) and megakaryocyte erythroid progenitors (MEPs) (Akashi et al., 2000) isolated from the bone marrow of young adult mice (Figures 1A and S1A).

Unfortunately, it is not possible to develop western blots with all ubiquitylated protein within the linear range of exposure, which precludes accurate quantification. To circumvent this limitation, we quantified ubiquitylated protein by intracellular flow cytometry using an antibody that preferentially recognizes polyubiquitin chains and exhibits no immunoreactivity with free ubiquitin (Markmiller et al., 2019). HSCs contained significantly less ubiquitylated protein than CMPs (47%; $p < 0.01$), GMPs (157%; $p < 0.001$), and MEPs (57%; $p < 0.001$) (Figures 1B and 1C).

Differences in ubiquitylated protein could not be explained by differences in cell volume, total protein abundance, or proteasome activity. Cell volume was similar between HSCs and CMPs (Figure 1D) despite HSCs having significantly less ubiquitylated protein (Figure 1B). Restricted progenitors also contained similar amounts of total protein as HSCs (Figure 1E and 1F), and HSCs had significantly less ubiquitylated protein than restricted progenitors even when normalized to total protein abundance (Figure 1G). HSCs also exhibited much less proteasome activity than CMPs (10-fold; $p < 0.001$), GMPs (132-fold; $p < 0.001$) (Signer et al., 2016), and MEPs (6.5-fold; $p < 0.01$) (Figure 3F).

Although ubiquitylated protein is used as a surrogate to quantify misfolded and unfolded proteins (Lee et al., 2006; Sontag et al., 2014; Vilchez et al., 2012), not all ubiquitylated protein arises from misfolding events. We thus sought an orthogonal assay to measure protein quality. Tetraphenylethene maleimide (TMI) is a cell-permeable dye that fluoresces upon binding to cysteine thiols (Chen et al., 2017). The free thiol side chains of non-disulphide-bonded hydrophobic cysteines are typically buried within the core of globular proteins (Marino and Gladyshev, 2010) but can be exposed in unfolded proteins (Figure 1H). We adapted TMI to quantify unfolded proteins within single hematopoietic cells by flow cytometry. Hematopoietic cells treated with TMI exhibited a clear increase in fluorescence relative to untreated controls (Figure S1B). Although glutathione represents a major pool of non-protein thiols within cells, it does not induce TMI fluorescence (Chen et al., 2017). Furthermore, glutathione levels do not significantly differ between HSCs and restricted progenitors (Agathocleous et al., 2017).

To validate TMI fluorescence as a reporter of unfolded protein accumulation in hematopoietic cells, we performed several independent experiments. First, we assessed the effect of heat shock, which induces protein unfolding (Morimoto, 2011), on TMI fluorescence in bone marrow cells. Bone marrow cells incubated at 42°C for 4 h exhibited a 22% increase in TMI fluorescence relative to an aliquot of the same cells incubated at 37°C (Figures 1I and S1B; $p < 0.05$). Heat-shocked bone marrow cells had statistically equivalent amounts of total protein

compared to bone marrow cells incubated at 37°C (Figure 1J), indicating that differences in TMI fluorescence do not simply reflect differences in total protein abundance. Next, because unfolded proteins are primarily degraded by the proteasome, we assessed the effects of proteasome inhibition on TMI fluorescence *in vivo*. Bone marrow cells isolated from mice treated with the proteasome inhibitor bortezomib exhibited a ~30% increase in TMI fluorescence compared to cells from vehicle-treated controls (Figures 1K and S1C; $p < 0.05$). Finally, we compared levels of ubiquitylated protein within TMI^{low} (lowest quartile of TMI fluorescence), TMI^{high} (highest quartile of TMI fluorescence), and unfractionated bone marrow cells by western blot. TMI^{low} bone marrow cells contained less ubiquitylated protein than unfractionated bone marrow cells, which in turn contained less ubiquitylated protein than TMI^{high} bone marrow cells (Figure S1D). These data suggest that TMI fluorescence accurately reflects the amount of unfolded proteins within primary hematopoietic cells.

The mean fluorescence intensity of TMI was significantly lower in HSCs than CMPs (32%; $p < 0.01$), GMPs (25%; $p < 0.05$), and MEPs (48%; $p < 0.01$) (Figures 1L and S1E–S1K). Although these differences appear rather modest, the increase in TMI fluorescence in restricted progenitors compared to HSCs was similar or greater in magnitude to that observed in bone marrow cells following either heat shock (Figure 1I) or bortezomib administration (Figure 1K), which are both treatments that significantly disrupt proteostasis. Overall, these data suggest that HSCs contain significantly elevated proteome quality compared to restricted myeloid progenitors *in vivo*.

Increasing Protein Synthesis Reduces Protein Quality within HSCs *In Vivo*

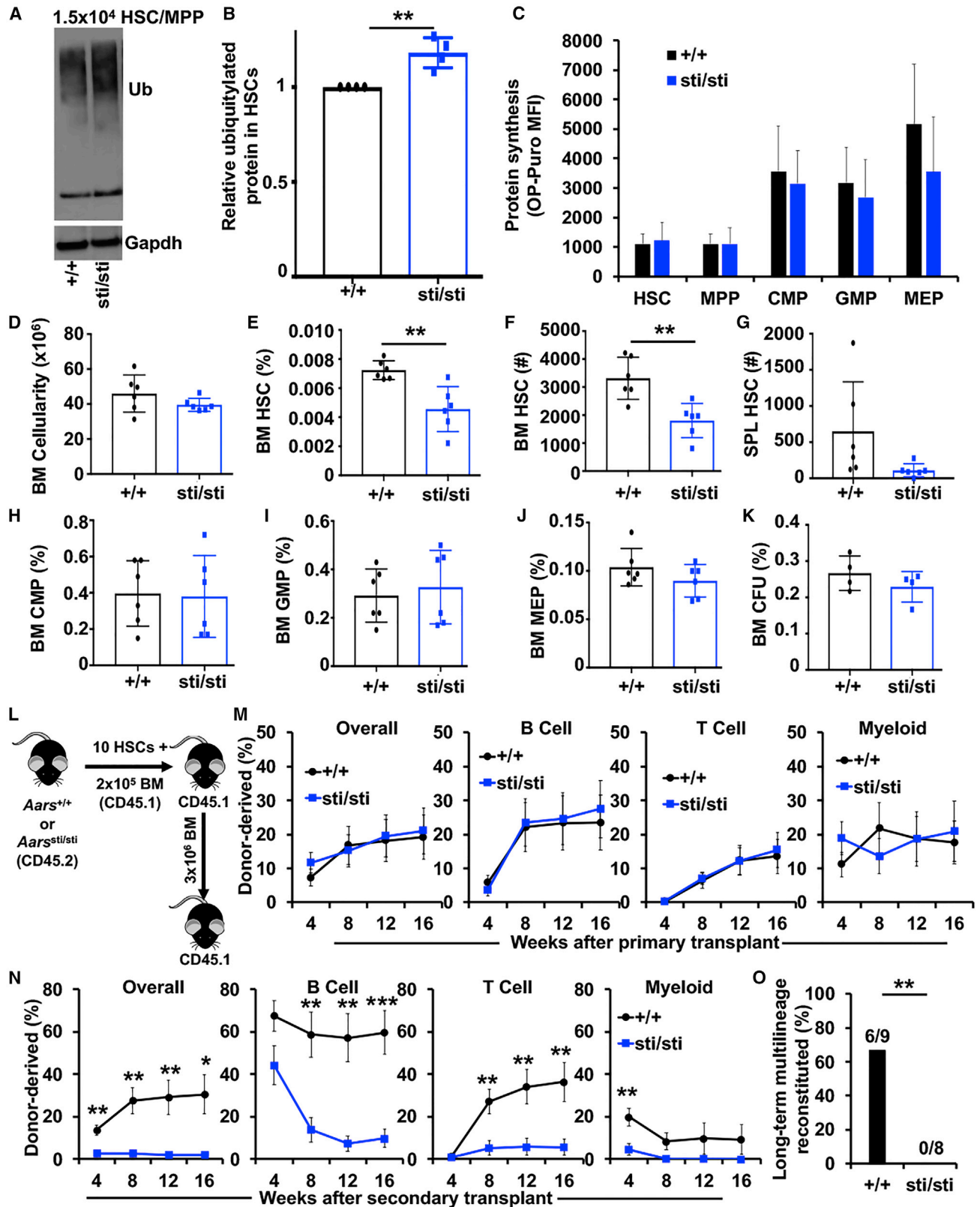
Adult HSCs exhibit unusually low protein synthesis compared to other hematopoietic cells (Figure 1M; Hidalgo San Jose and Signer, 2019; Signer et al., 2014). Translation is the most error-prone step in gene expression, and 10%–30% of all newly synthesized proteins are ubiquitylated and targeted for degradation (Lykke-Andersen and Bennett, 2014; Schubert et al., 2000). This raises the question of whether low protein synthesis in HSCs contributes to their reduced abundance of ubiquitylated and unfolded protein *in vivo*.

To test if increasing protein synthesis reduces proteome quality within HSCs, we took advantage of two genetic mouse models that modestly alter protein synthesis rates within HSCs *in vivo*. Conditional deletion of *Pten* from adult hematopoietic cells in *Mx1-Cre;Pten^{fl/fl}* mice leads to hyperactivation of the PI3K and mTOR signaling pathways, which increases protein synthesis by ~30% in HSCs (Signer et al., 2014). Introduction of a ribosomal mutation (*Rpl24^{Bst/+}*) (Oliver et al., 2004) functionally blocks this increase in protein synthesis within *Pten*-deficient HSCs without reducing hyperactivation of the downstream signaling pathways (Figure 1N; Signer et al., 2014). Increased protein synthesis within *Pten*-deficient HSCs was accompanied

(O) Western blot examining ubiquitylated protein in 8.5×10^3 HSCs/MPPs from *Pten^{fl/fl};Rpl24^{+/+}*, *Mx1-Cre⁺;Pten^{fl/fl};Rpl24^{+/+}*, and *Mx1-Cre⁺;Pten^{fl/fl};Rpl24^{Bst/+}* mice (one of 3 blots).

(P) TMI fluorescence in wild-type, *Mx1-Cre⁺;Pten^{fl/fl};Rpl24^{+/+}*, and *Mx1-Cre⁺;Pten^{fl/fl};Rpl24^{Bst/+}* mice ($n = 3–4$ mice/genotype).

Data represent mean \pm standard deviation. Statistical significance was assessed using a Student's t test (I–K) or an ANOVA followed by Dunnett's multiple comparisons test relative to HSCs (B, D, F, G, L, M, and P). * $p < 0.05$; ** $p < 0.01$; *** $p < 0.001$.



(legend on next page)

by an accumulation of ubiquitylated (Figure 1O) and unfolded protein (Figure 1P; ~30%; $p < 0.05$) relative to controls. *Rpl24*^{Bst/+}, which blocks the increase in protein synthesis (Signer et al., 2014), also blocked the increase in ubiquitylated and unfolded protein in *Pten*-deficient HSCs (Figures 1O and 1P). These data indicate that increased protein synthesis reduces protein quality within HSCs *in vivo* and suggests that HSCs depend upon low protein synthesis to maintain the integrity of their proteome.

Defects in tRNA Editing Preferentially Impair HSC Self-Renewal

We previously demonstrated that conditional deletion of *Pten* increases protein synthesis and severely impairs HSC function. Blocking the increase in protein synthesis with the *Rpl24*^{Bst/+} mutation largely rescues the function of *Pten*-deficient HSCs (Signer et al., 2014). These data indicate that increased protein synthesis impairs HSC function. Consistent with these observations, other genetic interventions that modestly increase protein synthesis within HSCs, such as deletion of *Eif4ebp1* and *Eif4ebp2* (Signer et al., 2016) or deletion of *Angiogenin* (Goncalves et al., 2016), also impair HSC function.

Given that increased protein synthesis impairs HSC function and reduces proteome quality (Figures 1O and 1P), it raised the question of whether the accumulation of misfolded and unfolded proteins contributes to HSC dysfunction. To test this, we sought a mouse model that could decouple increased protein synthesis and reduced protein quality. *Aars*^{sti/sti} mice harbor a mutation in the alanyl-tRNA synthetase that causes a tRNA editing defect that increases amino acid misincorporation at alanine residues, which can lead to an accumulation of mistranslated and ubiquitylated proteins within slowly and non-dividing cells (Lee et al., 2006). *Aars*^{sti/sti} mice exhibit some skin and hair texture defects as well as age-related neurological defects (Lee et al., 2006). Despite these defects, *Aars*^{sti/sti} mice are otherwise grossly normal and survive into adulthood. *Aars*^{sti/sti} HSCs had an 18% increase in ubiquitylated protein compared to littermate control HSCs (Figures 2A and 2B; $p < 0.01$). Notably, the accumulation of ubiquitylated protein in *Aars*^{sti/sti} HSCs occurred without significant changes in overall protein synthesis

(Figure 2C), cell size (Figure S2A) or proteasome activity (Figure 3I). Furthermore, the increase in ubiquitylated protein within *Aars*^{sti/sti} HSCs was within the physiological range observed within restricted progenitors (Figure S3A), making *Aars*^{sti/sti} HSCs more similar to other hematopoietic cells. These data establish *Aars*^{sti/sti} mice as a model to study the effects of a physiological decline in protein quality *in vivo* that is independent of changes in protein synthesis rate.

To assess the effects of reduced protein quality on hematopoiesis, we analyzed 8-week-old *Aars*^{sti/sti} and littermate control mice. *Aars*^{sti/sti} mice had normal bone marrow cellularity (Figure 2D) but significantly reduced spleen cellularity (Figure S2I) compared to controls. The frequency and absolute numbers of HSCs were significantly reduced by ~40% in the bone marrow of *Aars*^{sti/sti} mice (Figures 2E and 2F; $p < 0.01$). The decline in HSCs was not due to mobilization to the spleen, as *Aars*^{sti/sti} mice did not exhibit an increase in spleen HSCs (Figure 2G). In contrast to HSCs, the frequencies of CMPs, GMPs, MEPs, CD71⁺Ter119⁺ erythroid progenitors, CD11b⁺Gr1⁺ myeloid cells, pro-B cells, pre-B cells, IgM⁺ B cells, CD4⁺ T cells, and CD8⁺ T cells were unchanged in the bone marrow and spleen of *Aars*^{sti/sti} mice compared to controls (Figures 2H–2J and S2B–S2P). The frequency of colony-forming progenitors was also unchanged in *Aars*^{sti/sti} mice (Figure 2K). These data indicate that reduced protein quality in *Aars*^{sti/sti} mice impairs the maintenance of HSCs but does not significantly impact the maintenance of restricted hematopoietic progenitors.

To test if reduced protein quality impairs HSC function, we performed serial long-term reconstitution assays. We competitively transplanted 10 CD150⁺CD48[−]LSK HSCs from *Aars*^{sti/sti} or littermate control mice (CD45.2⁺) together with 2 × 10⁵ wild-type congenic (CD45.1⁺) bone marrow cells into lethally irradiated mice (CD45.1⁺) (Figure 2L). Overall, long-term hematopoietic reconstitution from *Aars*^{sti/sti} HSCs was statistically indistinguishable from controls in primary recipients (Figure 2M). After 16 weeks, 3 × 10⁶ bone marrow cells from primary recipient mice were serially transplanted into lethally irradiated mice. Secondary recipients of *Aars*^{sti/sti} HSCs exhibited significantly less donor cell reconstitution after transplantation (Figure 2N). None (0/8) of the secondary recipients of *Aars*^{sti/sti} HSCs exhibited long-term multilineage reconstitution compared to 67% (6/9) of

Figure 2. A tRNA Editing Defect that Reduces Proteome Quality Impairs HSC Self-Renewal

- (A) Western blot examining ubiquitylated protein in 2.5 × 10⁴ wild-type (+/+) and *Aars*^{sti/sti} (sti/sti) HSCs/MPPs, CMPs, GMPs, and MEPs (one of 2 blots).
 (B) Flow cytometry analysis showing ubiquitylated protein content in *Aars*^{sti/sti} (sti/sti) relative to wild-type (+/+) HSCs (n = 4 mice/genotype).
 (C) OP-Puro incorporation by wild-type (+/+) and *Aars*^{sti/sti} (sti/sti) HSCs and progenitor cells *in vivo* (n = 3 mice/genotype).
 (D) Bone marrow cellularity (BM; 1 femur and 1 tibia) in wild-type (+/+) and *Aars*^{sti/sti} (sti/sti) mice (n = 6 mice/genotype).
 (E) Frequency of HSCs in wild-type (+/+) and *Aars*^{sti/sti} (sti/sti) bone marrow (n = 6 mice/genotype).
 (F and G) Absolute number of HSCs in the bone marrow (1 femur and 1 tibia; F) and spleen (G) of wild-type (+/+) and *Aars*^{sti/sti} (sti/sti) mice (n = 6 mice/genotype).
 (H–J) Frequency of CMPs (H), GMPs (I), and MEPs (J) in wild-type (+/+) and *Aars*^{sti/sti} (sti/sti) bone marrow (n = 6 mice/genotype).
 (K) Frequency of colony-forming unit (CFU) progenitors in wild-type (+/+) and *Aars*^{sti/sti} (sti/sti) bone marrow (n = 4 mice/genotype).
 (L) Diagram showing HSC transplantation strategy.
 (M) Donor cell engraftment when 10 HSCs from wild-type (+/+) and *Aars*^{sti/sti} (sti/sti) mice were transplanted with 2 × 10⁵ recipient-type bone marrow cells into irradiated mice. Total hematopoietic cell, B cell, T cell, and myeloid cell engraftment is shown (n = 4 donors and 14–21 total recipients/genotype).
 (N) Donor cell engraftment in secondary recipients (n = 2 donors and 8–9 total recipients/genotype).
 (O) Frequency of secondary recipients in (N) that exhibited long-term (16-week) multilineage reconstitution (≥0.5% donor derived peripheral blood B, T, and myeloid cells).

Data represent mean ± standard deviation (B–K) or standard error of the mean (M and N). Statistical significance was assessed using a Student's t test or a Fisher's exact test (O). * $p < 0.05$; ** $p < 0.01$; *** $p < 0.001$.

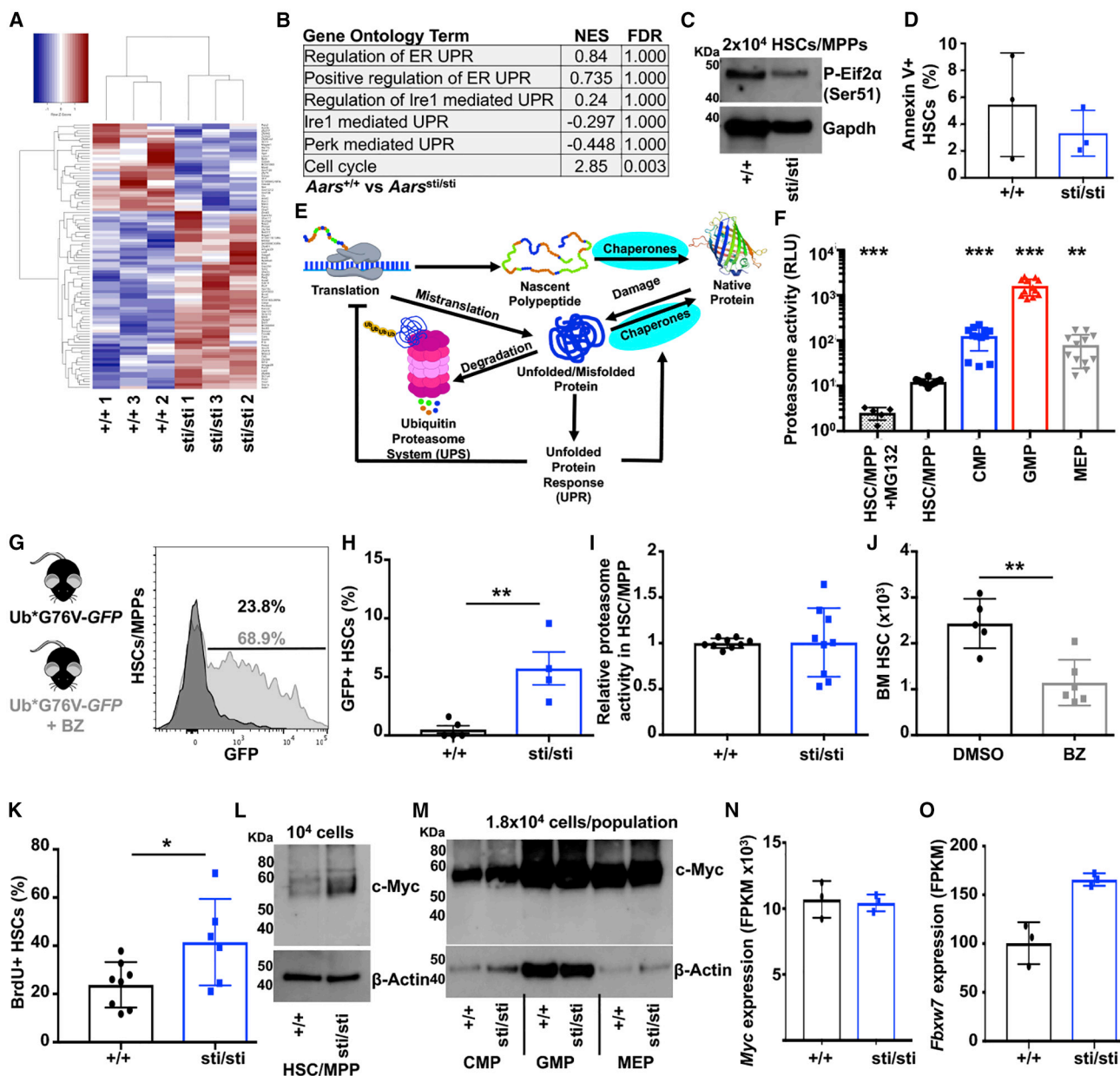


Figure 3. Accumulation of Ubiquitylated Protein Overwhelms the Proteasome in *Aars*^{sti/sti} HSCs, Leading to c-Myc Stabilization

(A) Heatmap showing 94 differentially expressed transcripts (≥ 2 -fold change; padj < 0.1) up- (red) or downregulated (blue) between wild-type (+/+) and *Aars*^{sti/sti} HSCs (n = 3 experiments/genotype).

(B) Gene set enrichment analysis demonstrating no significant activation of the UPR^{ER} in *Aars*^{sti/sti} HSCs.

(C) Western blot examining phosphorylated (Ser51)-Eif2 α in 2×10^4 wild-type (+/+) and *Aars*^{sti/sti} (sti/sti) HSCs/MPPs.

(D) Frequency of Annexin V⁺ HSCs in wild-type (+/+) and *Aars*^{sti/sti} (sti/sti) (n = 3 mice/genotype).

(E) Diagram of the proteostasis network.

(F) Proteasome activity in 5×10^3 HSCs/MPPs, CMPs, GMPs, and MEPs (n = 5–9 replicates in 4 experiments). Data are shown in relative luminescence units (RLUs).

(G) Representative histogram showing GFP expression in Ub^{G76V}-GFP HSCs/MPPs *in vitro* treated for 18 h with (gray) or without (black) BZ.

(H) Frequency of HSCs that are GFP⁺ in Ub^{G76V}-GFP (+/+) and Ub^{G76V}-GFP;*Aars*^{sti/sti} (sti/sti) bone marrow (n = 4–5 mice/genotype).

(I) Relative proteasome activity in wild-type (+/+) and *Aars*^{sti/sti} (sti/sti) HSCs/MPPs (n = 9 replicates in 3 experiments).

(J) Number of HSCs in the bone marrow (1 femur and 1 tibia) in mice treated with BZ or vehicle (DMSO) (n = 5–6 mice/treatment).

(K) Frequency of wild-type (+/+) and *Aars*^{sti/sti} (sti/sti) HSCs that incorporated BrdU after a 72-h pulse *in vivo* (n = 6–8 mice/genotype).

(L and M) Western blot examining c-Myc protein in 10^4 HSCs/MPPs (L) or 1.8×10^4 CMPs, GMPs and MEPs (M) isolated from wild-type (+/+) and *Aars*^{sti/sti} (sti/sti) mice (one of 2 (L) or 3 (M) blots).

(legend continued on next page)

controls (Figure 2O; $p < 0.01$). These data indicate that *Aars*^{sti/sti} HSCs have impaired self-renewal potential *in vivo*.

We next sought to determine whether reduced proteome quality preferentially impaired HSC function or whether it also impaired the function of restricted progenitors. In contrast to HSCs, we observed no significant increase in ubiquitylated protein among *Aars*^{sti/sti} myeloid progenitors (Figures S3A–S3D). This observation is consistent with previous reports that rapidly dividing cells efficiently dilute out misfolded proteins (Lee et al., 2006). Because *Aars*^{sti/sti} myeloid progenitors do not accumulate more ubiquitylated proteins than controls, we are precluded from making direct conclusions on the effect of reduced protein quality within those populations. We thus tested whether CD150⁺CD48⁺LSK MPPs (short-term HSCs), a progenitor cell population with similar cycling kinetics as HSCs (Oguro et al., 2013), would be susceptible to an accumulation of ubiquitylated proteins. Indeed, similar to HSCs, *Aars*^{sti/sti} MPPs exhibited a significant ~16% increase in ubiquitylated protein compared to controls (Figure S3E; $p < 0.05$). However, in contrast to HSCs, we observed no significant change in MPP frequency (Figure S3F). To test MPP function, we competitively transplanted 50 *Aars*^{sti/sti} or control MPPs into irradiated mice (Figure S3G). Levels of reconstitution by *Aars*^{sti/sti} MPPs were indistinguishable from controls (Figure S3H). Although HSC defects largely appeared during serial transplantation, it is not possible to perform secondary transplants with MPPs because they lack serial reconstituting activity. Nevertheless, these data suggest that HSCs are particularly sensitive to disruptions in proteostasis, as modest declines in protein quality preferentially impair HSC self-renewal.

Accumulation of Misfolded Proteins Overwhelms and/or Impairs the Proteasome in HSCs

An accumulation of misfolded and unfolded proteins can activate proteotoxic stress response pathways, including the endoplasmic reticulum unfolded protein response (UPR^{ER}) (Walter and Ron, 2011). Basal activity of the UPR^{ER} can promote HSC survival and engraftment (Chapple et al., 2018; Liu et al., 2019; van Galen et al., 2018). Under more severe stress conditions, activation of the UPR^{ER} can induce apoptosis within HSCs (van Galen et al., 2014) and fetal HSC self-renewal depends upon bile acids to suppress UPR^{ER} activation (Sigurdsson et al., 2016). This raised the question of whether the reduced HSC number in *Aars*^{sti/sti} mice was a consequence of activation of the UPR^{ER} and increased cell death. To test this, we performed RNA sequencing on *Aars*^{sti/sti} and control HSCs (Figure 3A) and looked for changes in the expression of gene sets related to the UPR^{ER}. We observed no significant changes in the expression of UPR^{ER}-related gene sets in *Aars*^{sti/sti} compared to control HSCs (Figure 3B). Consistent with this observation, *Aars*^{sti/sti} HSCs did not exhibit increased abundance of phosphorylated (Ser51) Eif2 α (Figure 3C), which is one marker of UPR^{ER} activation (Har-

ding et al., 1999). In addition, there was no significant difference in the frequency of Annexin V⁺ HSCs between *Aars*^{sti/sti} and control mice (Figure 3D), indicating that reduced HSC numbers in *Aars*^{sti/sti} mice are not due to increased cell death.

In the absence of detectable UPR^{ER} activation, we sought to uncover other potential mechanisms contributing to *Aars*^{sti/sti} HSC dysfunction. Proteostasis, in addition to protein biogenesis, is maintained by an integrated network of physiological mechanisms that promote protein folding, repair, and degradation (Labbadia and Morimoto, 2015; Figure 3E). Previous work has demonstrated that overexpression of aggregation-prone proteins can overwhelm and/or impair the ubiquitin proteasome system in HEK293 cells (Bence et al., 2001). Because HSCs exhibited less proteasome activity than restricted progenitors (Figure 3F), we hypothesized that an accumulation of misfolded proteins might overwhelm the capacity of the proteasome within HSCs to efficiently degrade all ubiquitylated substrates.

To test this, we used Ub^{G76V}-GFP proteasome reporter mice (Lindsten et al., 2003). Ub^{G76V}-GFP mice ubiquitously express GFP that is fused to a constitutive degradation signal. GFP transcripts can be detected in various tissues, but no GFP fluorescence is detected because the protein is rapidly degraded by the proteasome. However, administration of a proteasome inhibitor leads to robust GFP fluorescence (Figure 3G; Lindsten et al., 2003). Similar to other cell types, Ub^{G76V}-GFP HSCs did not express significant GFP fluorescence *in vivo* (Figure 3H). We crossed Ub^{G76V}-GFP mice to *Aars*^{sti/sti} mice and assessed GFP expression within HSCs. Strikingly, we observed a significant accumulation of GFP⁺ HSCs within Ub^{G76V}-GFP;*Aars*^{sti/sti} mice (Figure 3H; $p < 0.01$), and this was not due to a reduction in proteasome activity (Figure 3I). These data indicate that the proteasome can become overwhelmed and/or impaired when misfolded proteins accumulate within HSCs.

To test if insufficient proteasome activity impairs HSC maintenance, we treated mice with bortezomib for 3 consecutive days and assessed HSC numbers in the bone marrow on day 4. Mice treated with bortezomib exhibited a ~50% reduction in HSCs compared to vehicle (DMSO)-treated controls (Figure 3J; $p < 0.01$). The bortezomib-mediated decline in HSCs was similar to the decline in HSCs observed within *Aars*^{sti/sti} mice (Figure 2F). These data indicate that impaired proteasome activity impairs HSC maintenance and suggest that the decline in *Aars*^{sti/sti} HSCs may be caused by their overwhelmed/impaired proteasome.

Accumulation of Misfolded Proteins Is Associated with c-Myc Accumulation in HSCs

In addition to regulating proteostasis, the ubiquitin proteasome system post-translationally regulates the abundance of multiple proteins that affect diverse cellular functions, including HSC fate (Moran-Crusio et al., 2012). As a consequence, we wondered if overwhelming the proteasome might lead to stabilization of

(N) *Myc* expression normalized to β -Actin in wild-type (+/+) and *Aars*^{sti/sti} (sti/sti) HSCs ($n = 3$).

(O) *Fbxw7* expression in wild-type (+/+) and *Aars*^{sti/sti} (sti/sti) HSCs ($n = 3$ /genotype).

Data represent mean \pm standard deviation. Statistical significance was assessed using a Student's *t* test (D, H, I, J, K, N, and O) or an ANOVA followed by Dunnett's test relative to HSCs/MPPs (F). * $p < 0.05$; ** $p < 0.01$; *** $p < 0.001$.

some of these proteasome targets within HSCs. Our RNA sequencing data revealed a significant increase in the expression of cell cycle genes within *Aars*^{sti/sti} HSCs (Figure 3B). In accordance with these gene expression studies, we determined that *Aars*^{sti/sti} HSCs exhibited increased proliferation *in vivo* compared to controls. After a 72-h pulse of bromodeoxyuridine (BrdU) *in vivo*, 41.5% of *Aars*^{sti/sti} HSCs incorporated BrdU compared to 23.8% of control HSCs (Figure 3K; $p < 0.05$).

Because *Aars*^{sti/sti} HSCs exhibited increased proliferation (Figure 3K) and diminished self-renewal activity (Figures 2N and 2O), we sought to identify known proteasome-regulated targets that could contribute to these phenotypes. The target that we focused on was c-Myc. c-Myc has an established role in regulating HSC quiescence, cell cycle entry, and self-renewal. Although *Myc* is transcribed at similar levels in HSCs and progenitors, the c-Myc protein is mostly absent from HSCs but accumulates in more differentiated progenitors (Reavie et al., 2010). Conditional deletion of the E3 ubiquitin ligase *Fbxw7* leads to an accumulation of c-Myc protein within HSCs (Reavie et al., 2010; Thompson et al., 2008), suggesting that *Fbxw7* targets c-Myc for degradation. *Fbxw7*^{-/-} HSCs exhibit increased cycling and premature exhaustion (Matsuoka et al., 2008; Thompson et al., 2008), which is similar to HSCs with enforced expression of c-Myc (Wilson et al., 2004). Genetic inactivation of one allele of *Myc* is sufficient to partially rescue *Fbxw7*^{-/-} HSCs (Reavie et al., 2010). These studies indicate that proteasome-mediated degradation of c-Myc is essential for normal HSC quiescence and self-renewal.

Given that c-Myc is heavily regulated by the proteasome, promotes HSC cell cycle entry, and influences HSC self-renewal, we investigated whether c-Myc was dysregulated in *Aars*^{sti/sti} mice. We determined that *Aars*^{sti/sti} HSCs/MPPs expressed elevated amounts of c-Myc protein relative to controls (Figure 3L), but no such changes were evident within restricted progenitors (Figure 3M). The increase in the c-Myc protein could not be explained by increased *Myc* mRNA expression, which was unchanged within *Aars*^{sti/sti} HSCs (Figure 3N). Increased c-Myc expression also could neither be explained by reduced expression of *Fbxw7* nor any other E3 ubiquitin ligases implicated in c-Myc ubiquitylation (Figures 3O and S4H–S4S). Although we cannot rule out all possible mechanisms, our data suggest that c-Myc accumulates within *Aars*^{sti/sti} HSCs at least in part because of impaired degradation as a consequence of overwhelmed and/or impaired proteasome capacity.

To further support our findings in *Aars*^{sti/sti} HSCs, we tested whether an accumulation of misfolded and unfolded proteins had similar effects on proteasome capacity and c-Myc expression in *Pten*-deficient HSCs that accumulate ubiquitylated proteins as a consequence of increased protein synthesis (Figure 1O). Consistent with our observations in *Aars*^{sti/sti} HSCs, *Pten*-deficient HSCs exhibited a robust increase in c-Myc protein expression (Figure S4B) without any increase in *Myc* mRNA expression (Figure S4C) or decline in *Fbxw7* expression (Figure S4D). In addition, we observed a significant increase in GFP⁺ HSCs within *Mx1-Cre*⁺;*Pten*^{fl/fl};*UB*^{G76V}-GFP mice (Figure S4E), indicating that *Pten*-deficient HSCs also experience an overwhelming or impairment of their proteasome without any significant change in overall proteasome capacity (Fig-

ure S4F). Notably, the *Rpl24*^{Bst/+} mutation reduced the abundance of c-Myc in *Pten*-deficient HSCs/MPPs to near wild-type levels (Figure S4G). Taken together, these data strongly suggest that a modest accumulation of misfolded proteins is sufficient to overwhelm the capacity of the proteasome within HSCs and is associated with accumulation of c-Myc.

Reducing c-Myc Expression Partially Rescues Self-Renewal Defects in *Aars*^{sti/sti} HSCs

Because c-Myc overexpression can impair HSC self-renewal, we hypothesized that c-Myc accumulation within *Aars*^{sti/sti} HSCs was contributing to defects in serial reconstituting activity. To test this, we sought to reduce c-Myc expression within *Aars*^{sti/sti} HSCs. We could not completely delete *Myc* because *Myc* deficiency causes severe hematopoietic defects (Wilson et al., 2004). We, thus, sought to reduce c-Myc expression by conditionally deleting a single allele of *Myc* in *Aars*^{sti/sti} mice by breeding *Mx1-Cre*⁺;*Myc*^{fl/+};*Aars*^{sti/sti} (*Aars*^{sti/sti};*Myc*^{+/-}) mice. Remarkably, c-Myc expression in *Aars*^{sti/sti} HSCs was reduced to near wild-type levels in *Aars*^{sti/sti};*Myc*^{+/-} HSCs (Figure 4A), whereas levels of ubiquitylated protein were still elevated (data not shown).

To test if reducing c-Myc expression could partially rescue *Aars*^{sti/sti} HSC self-renewal, we performed serial long-term reconstitution assays. We competitively transplanted 5×10^5 *Mx1-Cre*⁺;*Myc*^{fl/+};*Aars*^{sti/sti}, *Aars*^{sti/sti} or wild-type control bone marrow cells (CD45.2⁺) together with 5×10^5 congenic bone marrow cells (CD45.1⁺) into lethally irradiated mice (CD45.1⁺) (Figure 4B). Similar to our HSC transplants (Figure 2M), long-term hematopoietic reconstitution from *Aars*^{sti/sti} bone marrow cells was statistically indistinguishable from controls in primary recipients (Figure 4C). *Aars*^{sti/sti};*Myc*^{+/-} bone marrow cells also gave similar levels of reconstitution in primary transplants, although they did exhibit a slight, but significant reduction in B cell reconstitution. After 16 weeks, 3×10^6 bone marrow cells from primary recipient mice were serially transplanted into lethally irradiated mice. Secondary recipients of *Aars*^{sti/sti} bone marrow cells exhibited significantly less donor cell reconstitution in all lineages after transplantation (Figure 4D). Strikingly, reducing c-Myc expression in *Aars*^{sti/sti};*Myc*^{+/-} HSCs partially prevented these defects (Figure 4D). *Aars*^{sti/sti};*Myc*^{+/-} cells gave similar levels of reconstitution as wild-type cells, except in the B cell lineage where reconstitution was still reduced (Figure 4D). Overall, long-term multilineage reconstitution in secondary transplants was reduced from 95% (35/37) in recipients of wild-type cells to 39% (17/44) in recipients of *Aars*^{sti/sti} cells ($p < 0.001$), but was increased back to 94% (16/17) in recipients of *Aars*^{sti/sti};*Myc*^{+/-} cells (Figure 4E; $p < 0.001$). These data indicate that reducing c-Myc expression partially prevents self-renewal defects within *Aars*^{sti/sti} HSC, and suggest that c-Myc accumulation contributes to impaired HSC function when proteostasis is perturbed.

DISCUSSION

Low protein synthesis is a broadly conserved feature of somatic stem cells (Blanco et al., 2016; Llorens-Bobadilla et al., 2015; Sanchez et al., 2016; Signer et al., 2014; Zismanov

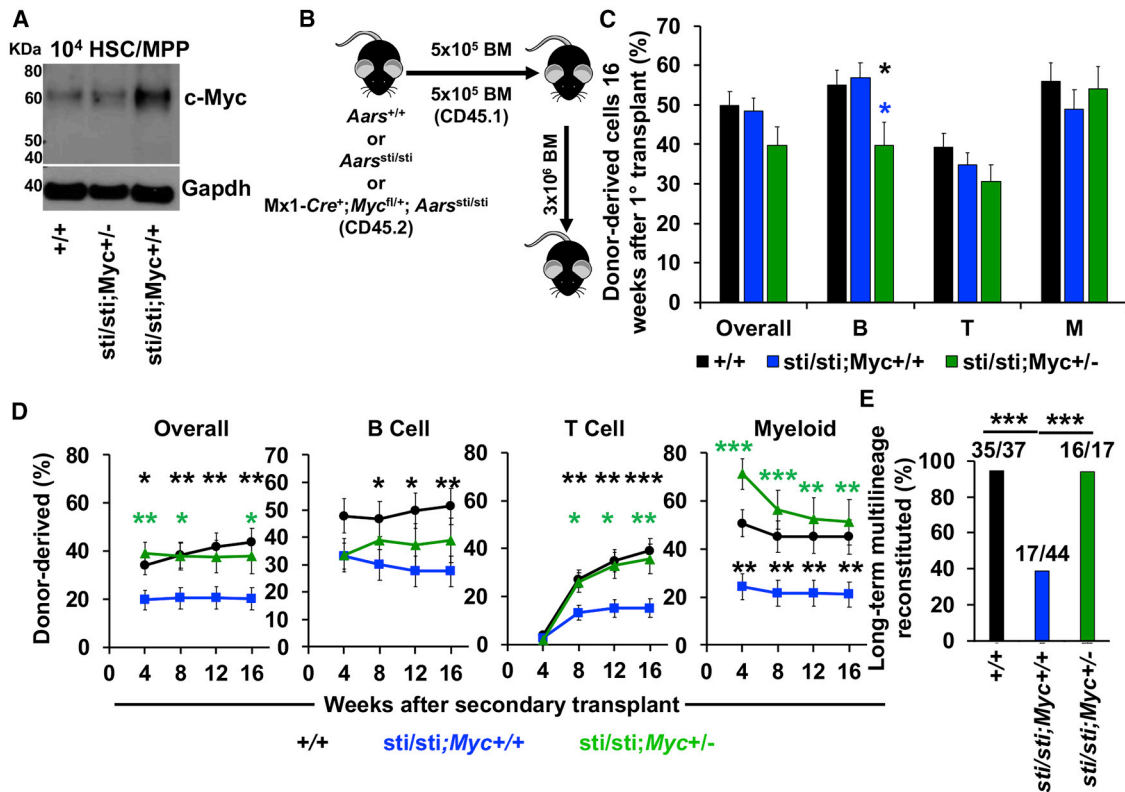


Figure 4. Reducing c-Myc Expression Largely Rescues Serial Reconstituting Activity of *Aars*^{sti/sti} HSCs

(A) Western blot examining c-Myc in 10⁴ HSCs/MPPs isolated from wild-type (+/+), Mx1-Cre⁺; *Aars*^{sti/sti}; *Myc*^{fl/+} (sti/sti;Myc+/-) and *Aars*^{sti/sti} (sti/sti;Myc+/+) mice. (B) Diagram showing bone marrow transplantation strategy. (C) Donor cell engraftment 16 weeks after 5 × 10⁵ bone marrow cells from wild-type (+/+), *Aars*^{sti/sti} (sti/sti;Myc+/+) and Mx1-Cre⁺; *Aars*^{sti/sti}; *Myc*^{fl/+} (sti/sti;Myc+/-) mice were transplanted with 5 × 10⁵ recipient-type bone marrow cells into irradiated mice. Total hematopoietic cells, B cell, T cell, and myeloid cell engraftment is shown (n = 4–8 donors and 26–44 total recipients/genotype). (D) Donor cell engraftment in secondary recipients (n = 4–10 donors and 17–44 recipients/genotype). (E) Frequency of secondary recipients in (D) that exhibited long-term multilineage reconstitution. Data represent mean ± standard error of the mean. Statistical significance was assessed using a Student's t test (C and D) or Fisher's exact test (E). *p < 0.05; **p < 0.01; ***p < 0.001.

et al., 2016) that promotes regeneration in multiple tissues. However, little is known about why stem cells depend upon low protein synthesis and why modest increases in protein synthesis impair stem cell function. In this study, we set out to address this question by examining the influence of protein synthesis on protein quality and homeostasis. We found that HSCs contain less ubiquitinated and unfolded protein than restricted myeloid progenitors *in vivo* (Figure 1) and that modest increases in protein synthesis reduce protein quality within HSCs. To investigate the consequences of reduced protein quality on HSCs independent of changes in protein synthesis rate, we examined *Aars*^{sti/sti} mice that have a defect in tRNA editing activity. The accumulation of defective translational products within *Aars*^{sti/sti} HSCs impaired their serial long-term multilineage reconstituting activity (Figure 2). Surprisingly, we found that the accumulation of misfolded proteins overwhelmed and/or impaired the proteasome and led to increased c-Myc abundance in both *Aars*^{sti/sti} and *Pten*-deficient HSCs (Figures 3 and S4). Reducing c-Myc expression by deleting a

single allele of *Myc* partially prevented the self-renewal defects observed in *Aars*^{sti/sti} HSCs (Figure 4). Overall, our studies indicate that stem cells depend upon low protein synthesis to maintain proteome quality and that modest accumulation of misfolded proteins preferentially impairs HSC self-renewal.

Our finding that the proteasome gets overloaded and impaired in HSCs raises the possibility that stem cells may depend on alternative mechanisms to detoxify and eliminate misfolded proteins. One possibility is that HSCs preferentially depend upon autophagy to degrade misfolded proteins. In support of this possibility, two recent studies reported that autophagy promotes proteostasis maintenance within aging neural stem cells (Lee-man et al., 2018) and muscle satellite cells (Garcia-Prat et al., 2016). Similar to HSCs, quiescent neural stem cells also contain less proteasome activity than restricted progenitors and neural stem cells preferentially store misfolded proteins as aggregates in lysosomes (Lee-man et al., 2018). Several studies have demonstrated an essential role for autophagy in HSCs (Ho et al., 2017; Liu et al., 2010; Mortensen et al., 2011; Warr et al., 2013), but to

our knowledge, whether autophagy promotes proteostasis maintenance within HSCs is unstudied.

In addition to degradation pathways, HSCs could eliminate misfolded proteins through proliferation. Cell division enables cells to dilute out misfolded proteins by distributing them to daughter cells. We determined that a buildup of misfolded proteins led to an accumulation of c-Myc and increased proliferation in HSCs but not restricted progenitors (Figure 3). These data reveal a stem-cell-specific molecular mechanism connecting the proteostasis network to cell cycle control. An intriguing possibility is that HSCs sense changes in protein synthesis and homeostasis by proteasome-mediated turnover of c-Myc, and c-Myc accumulation could be an adaptive mechanism used by individual HSCs to restore proteostasis within daughter stem cells generated by self-renewing divisions. Furthermore, this mechanism could also protect the HSC pool because HSCs unable to restore proteostasis would have sustained c-Myc expression, which promotes HSC differentiation (Wilson et al., 2004).

c-Myc is not the only protein in HSCs whose expression is regulated by the proteasome (Moran-Crusio et al., 2012). Interestingly, a previous report determined that expression of p53, which is also heavily regulated by the proteasome in HSCs (Abbas et al., 2010), is elevated within *Pten*-deficient HSCs and contributes to self-renewal defects in that background (Lee et al., 2010). Deleting a single allele of *Myc* also modestly restores long-term multilineage, reconstituting activity within *Pten*-deficient HSCs (data not shown). Overwhelming of the proteasome due to an accumulation of misfolded and unfolded proteins is likely to have more widespread effects on HSC proteome content. However, detailed proteomic analyses needed to broadly investigate this possibility remain technically difficult to perform within rare HSCs.

Disrupted proteostasis is a hallmark of aging (López-Otín et al., 2013), but whether it contributes to HSC aging is still untested. An intriguing possibility is that disrupted proteostasis in aging HSCs could contribute to HSC dysfunction and the increased incidence of blood cancer in the elderly by preventing the degradation of c-Myc. A potential role for c-Myc in stem cell aging could extend a recent study that demonstrated that reducing *Myc* expression enhances longevity in mice (Hofmann et al., 2015).

Low protein synthesis is a shared feature of many types of somatic stem cells (Blanco et al., 2016; Llorens-Bobadilla et al., 2015; Sanchez et al., 2016; Signer et al., 2014; Zismanov et al., 2016). Our findings raise the possibility that the maintenance of proteostasis is similarly required by stem cells in diverse tissues. Interestingly, interventions that reduce protein synthesis and enhance proteostasis extend organismal lifespan in an evolutionarily conserved manner (Taylor and Dillin, 2011). Our current findings suggest that mechanisms that promote organismal longevity are conserved at the cellular level to maintain long-lived stem cells *in vivo*.

STAR★METHODS

Detailed methods are provided in the online version of this paper and include the following:

- KEY RESOURCES TABLE
- LEAD CONTACT AND MATERIALS AVAILABILITY
- EXPERIMENTAL MODEL AND SUBJECT DETAILS
 - Mice
 - Cell isolation
- METHOD DETAILS
 - PIPC treatment
 - Proteasome inhibition
 - Flow cytometry and sorting
 - Competitive repopulation assay
 - Western blot analysis
 - Measurement of unfolded proteins
 - *In vivo* measurement of protein synthesis
 - *In vitro* analysis
 - Cell volume
 - Protein content
 - Proteasome activity
 - RNA sequencing
 - Quantitative PCR
- QUANTIFICATION AND STATISTICAL ANALYSIS
- DATA AND CODE AVAILABILITY

SUPPLEMENTAL INFORMATION

Supplemental Information can be found online at <https://doi.org/10.1016/j.celrep.2019.12.003>.

ACKNOWLEDGMENTS

We would like to thank E.J. Bennett, M. Leonard, S.A. Ackerman, J.S. Gutkind, S.J. Morrison, and J.A. Magee, C. Kim and the staff at the LJI Flow Cytometry core facility, J. Day and S. Wlodychak at the LJI NGS core facility, and J. Greenbaum and A. Chawla at the LJI Bioinformatics core facility. This work was supported by the NIH/NIDDK (R01DK116951), Scholar Awards from the V Foundation for Cancer Research (V2017-003) and the American Society of Hematology, the American Cancer Society Institutional Research Grant (IRG-15-172-45-IRG), the Sanford Stem Cell Clinical Center, and the UCSD Moores Cancer Center, which is supported by the NIH/NCI Specialized Cancer Center Support Grant (2P30CA023100-33). The LJI Flow Cytometry core facility is supported by the NIH Shared Instrumentation Grant Program (S10 RR027366). L.H.S.J. was supported by a Chancellor's Research Excellence Scholarship.

AUTHOR CONTRIBUTIONS

R.A.J.S. conceived the project and wrote the manuscript. L.H.S.J., M.J.S., C.H.D., B.A.C., M.K., and R.A.J.S. designed and performed the experiments, analyzed the data, and interpreted the results. Y.H. and D.M.H. developed the TMI reagent and edited the manuscript.

DECLARATION OF INTERESTS

The authors declare no competing financial interests.

Received: June 27, 2019

Revised: November 2, 2019

Accepted: November 27, 2019

Published: January 7, 2020

REFERENCES

Abbas, H.A., Maccio, D.R., Coskun, S., Jackson, J.G., Hazen, A.L., Sills, T.M., You, M.J., Hirschi, K.K., and Lozano, G. (2010). *Mdm2* is required for survival of

- hematopoietic stem cells/progenitors via dampening of ROS-induced p53 activity. *Cell Stem Cell* 7, 606–617.
- Agathocleous, M., Meacham, C.E., Burgess, R.J., Piskounova, E., Zhao, Z., Crane, G.M., Cowin, B.L., Bruner, E., Murphy, M.M., Chen, W., et al. (2017). Ascorbate regulates haematopoietic stem cell function and leukaemogenesis. *Nature* 549, 476–481.
- Akashi, K., Traver, D., Miyamoto, T., and Weissman, I.L. (2000). A clonogenic common myeloid progenitor that gives rise to all myeloid lineages. *Nature* 404, 193–197.
- Anders, S., Pyl, P.T., and Huber, W. (2015). HTSeq—a Python framework to work with high-throughput sequencing data. *Bioinformatics* 31, 166–169.
- Bence, N.F., Sampat, R.M., and Kopito, R.R. (2001). Impairment of the ubiquitin-proteasome system by protein aggregation. *Science* 292, 1552–1555.
- Blanco, S., Bandiera, R., Popis, M., Hussain, S., Lombard, P., Aleksic, J., Sajjini, A., Tanna, H., Cortés-Garrido, R., Gkatza, N., et al. (2016). Stem cell function and stress response are controlled by protein synthesis. *Nature* 534, 335–340.
- Chapple, R.H., Hu, T., Tseng, Y.J., Liu, L., Kitano, A., Luu, V., Hoegenauer, K.A., Iwawaki, T., Li, Q., and Nakada, D. (2018). ER α promotes murine hematopoietic regeneration through the Ire1 α -mediated unfolded protein response. *eLife* 7, e31159.
- Chen, M.Z., Moily, N.S., Bridgford, J.L., Wood, R.J., Radwan, M., Smith, T.A., Song, Z., Tang, B.Z., Tilley, L., Xu, X., et al. (2017). A thiol probe for measuring unfolded protein load and proteostasis in cells. *Nat. Commun.* 8, 474.
- de Alboran, I.M., O'Hagan, R.C., Gärtner, F., Malynn, B., Davidson, L., Rickert, R., Rajewsky, K., DePinho, R.A., and Alt, F.W. (2001). Analysis of C-MYC function in normal cells via conditional gene-targeted mutation. *Immunity* 14, 45–55.
- Drummond, D.A., and Wilke, C.O. (2009). The evolutionary consequences of erroneous protein synthesis. *Nat. Rev. Genet.* 10, 715–724.
- Duttler, S., Pechmann, S., and Frydman, J. (2013). Principles of cotranslational ubiquitination and quality control at the ribosome. *Mol. Cell* 50, 379–393.
- García-Prat, L., Martínez-Vicente, M., Perdiguer, E., Ortet, L., Rodríguez-Ubrea, J., Rebollo, E., Ruiz-Bonilla, V., Gutarra, S., Ballestar, E., Serrano, A.L., et al. (2016). Autophagy maintains stemness by preventing senescence. *Nature* 529, 37–42.
- Goncalves, K.A., Silberstein, L., Li, S., Severe, N., Hu, M.G., Yang, H., Scadden, D.T., and Hu, G.F. (2016). Angiogenin Promotes Hematopoietic Regeneration by Dichotomously Regulating Quiescence of Stem and Progenitor Cells. *Cell* 166, 894–906.
- Groszer, M., Erickson, R., Scripture-Adams, D.D., Dougherty, J.D., Le Belle, J., Zack, J.A., Geschwind, D.H., Liu, X., Kornblum, H.I., and Wu, H. (2006). PTEN negatively regulates neural stem cell self-renewal by modulating G0-G1 cell cycle entry. *Proc. Natl. Acad. Sci. USA* 103, 111–116.
- Harding, H.P., Zhang, Y., and Ron, D. (1999). Protein translation and folding are coupled by an endoplasmic-reticulum-resident kinase. *Nature* 397, 271–274.
- Hidalgo San Jose, L., and Signer, R.A.J. (2019). Cell-type-specific quantification of protein synthesis *in vivo*. *Nat. Protoc.* 14, 441–460.
- Ho, T.T., Warr, M.R., Adelman, E.R., Lansinger, O.M., Flach, J., Verovskaya, E.V., Figueroa, M.E., and Passequé, E. (2017). Autophagy maintains the metabolism and function of young and old stem cells. *Nature* 543, 205–210.
- Hofmann, J.W., Zhao, X., De Cecco, M., Peterson, A.L., Pagliaroli, L., Manivannan, J., Hubbard, G.B., Ikeno, Y., Zhang, Y., Feng, B., et al. (2015). Reduced expression of MYC increases longevity and enhances healthspan. *Cell* 160, 477–488.
- Kiel, M.J., Yilmaz, O.H., Iwashita, T., Yilmaz, O.H., Terhorst, C., and Morrison, S.J. (2005). SLAM family receptors distinguish hematopoietic stem and progenitor cells and reveal endothelial niches for stem cells. *Cell* 121, 1109–1121.
- Kim, W., Bennett, E.J., Huttlin, E.L., Guo, A., Li, J., Possemato, A., Sowa, M.E., Rad, R., Rush, J., Comb, M.J., et al. (2011). Systematic and quantitative assessment of the ubiquitin-modified proteome. *Mol. Cell* 44, 325–340.
- Kühn, R., Schwenk, F., Aguet, M., and Rajewsky, K. (1995). Inducible gene targeting in mice. *Science* 269, 1427–1429.
- Labbadia, J., and Morimoto, R.I. (2015). The biology of proteostasis in aging and disease. *Annu. Rev. Biochem.* 84, 435–464.
- Lee, J.W., Beebe, K., Nangle, L.A., Jang, J., Longo-Guess, C.M., Cook, S.A., Davisson, M.T., Sundberg, J.P., Schimmel, P., and Ackerman, S.L. (2006). Editing-defective tRNA synthetase causes protein misfolding and neurodegeneration. *Nature* 443, 50–55.
- Lee, J.Y., Nakada, D., Yilmaz, O.H., Tothova, Z., Joseph, N.M., Lim, M.S., Gilliland, D.G., and Morrison, S.J. (2010). mTOR activation induces tumor suppressors that inhibit leukemogenesis and deplete hematopoietic stem cells after Pten deletion. *Cell Stem Cell* 7, 593–605.
- Leeman, D.S., Hebestreit, K., Ruetz, T., Webb, A.E., McKay, A., Pollina, E.A., Dulken, B.W., Zhao, X., Yeo, R.W., Ho, T.T., et al. (2018). Lysosome activation clears aggregates and enhances quiescent neural stem cell activation during aging. *Science* 359, 1277–1283.
- Li, H., Handsaker, B., Wysoker, A., Fennell, T., Ruan, J., Homer, N., Marth, G., Abecasis, G., and Durbin, R.; 1000 Genome Project Data Processing Subgroup (2009). The Sequence Alignment/Map format and SAMtools. *Bioinformatics* 25, 2078–2079.
- Lindsten, K., Menéndez-Benito, V., Masucci, M.G., and Dantuma, N.P. (2003). A transgenic mouse model of the ubiquitin/proteasome system. *Nat. Biotechnol.* 21, 897–902.
- Liu, F., Lee, J.Y., Wei, H., Tanabe, O., Engel, J.D., Morrison, S.J., and Guan, J.L. (2010). FIP200 is required for the cell-autonomous maintenance of fetal hematopoietic stem cells. *Blood* 116, 4806–4814.
- Liu, L., Zhao, M., Jin, X., Ney, G., Yang, K.B., Peng, F., Cao, J., Iwawaki, T., Del Valle, J., Chen, X., and Li, Q. (2019). Adaptive endoplasmic reticulum stress signalling via IRE1 α -XBP1 preserves self-renewal of haematopoietic and pre-leukaemic stem cells. *Nat. Cell Biol.* 21, 328–337.
- Llorens-Bobadilla, E., Zhao, S., Baser, A., Saiz-Castro, G., Zwadlo, K., and Martín-Villalba, A. (2015). Single-Cell Transcriptomics Reveals a Population of Dormant Neural Stem Cells that Become Activated upon Brain Injury. *Cell Stem Cell* 17, 329–340.
- López-Otín, C., Blasco, M.A., Partridge, L., Serrano, M., and Kroemer, G. (2013). The hallmarks of aging. *Cell* 153, 1194–1217.
- Love, M.I., Huber, W., and Anders, S. (2014). Moderated estimation of fold change and dispersion for RNA-seq data with DESeq2. *Genome Biol.* 15, 550.
- Lykke-Andersen, J., and Bennett, E.J. (2014). Protecting the proteome: Eukaryotic cotranslational quality control pathways. *J. Cell Biol.* 204, 467–476.
- Marino, S.M., and Gladyshev, V.N. (2010). Cysteine function governs its conservation and degeneration and restricts its utilization on protein surfaces. *J. Mol. Biol.* 404, 902–916.
- Markmiller, S., Fulzele, A., Higgins, R., Leonard, M., Yeo, G.W., and Bennett, E.J. (2019). Active Protein Neddylolation or Ubiquitylation Is Dispensable for Stress Granule Dynamics. *Cell Rep.* 27, 1356–1363.e3.
- Matsuoka, S., Oike, Y., Onoyama, I., Iwama, A., Arai, F., Takubo, K., Mashimo, Y., Oguro, H., Nitta, E., Ito, K., et al. (2008). Fbxw7 acts as a critical fail-safe against premature loss of hematopoietic stem cells and development of T-ALL. *Genes Dev.* 22, 986–991.
- Moran-Crusio, K., Reavie, L.B., and Aifantis, I. (2012). Regulation of hematopoietic stem cell fate by the ubiquitin proteasome system. *Trends Immunol.* 33, 357–363.
- Morimoto, R.I. (2011). The heat shock response: systems biology of proteotoxic stress in aging and disease. *Cold Spring Harb. Symp. Quant. Biol.* 76, 91–99.
- Mortensen, M., Soilleux, E.J., Djordjevic, G., Tripp, R., Lutteropp, M., Sadighi-Akha, E., Stranks, A.J., Glanville, J., Knight, S., Jacobsen, S.E., et al. (2011). The autophagy protein Atg7 is essential for hematopoietic stem cell maintenance. *J. Exp. Med.* 208, 455–467.
- Oguro, H., Ding, L., and Morrison, S.J. (2013). SLAM family markers resolve functionally distinct subpopulations of hematopoietic stem cells and multipotent progenitors. *Cell Stem Cell* 13, 102–116.

- Oliver, E.R., Saunders, T.L., Tarlé, S.A., and Glaser, T. (2004). Ribosomal protein L24 defect in belly spot and tail (Bst), a mouse Minute. *Development* *131*, 3907–3920.
- Picelli, S., Faridani, O.R., Björklund, A.K., Winberg, G., Sagasser, S., and Sandberg, R. (2014). Full-length RNA-seq from single cells using Smart-seq2. *Nat. Protoc.* *9*, 171–181.
- Reavie, L., Della Gatta, G., Crusio, K., Aranda-Orgilles, B., Buckley, S.M., Thompson, B., Lee, E., Gao, J., Bredemeyer, A.L., Helmink, B.A., et al. (2010). Regulation of hematopoietic stem cell differentiation by a single ubiquitin ligase-substrate complex. *Nat. Immunol.* *11*, 207–215.
- Sanchez, C.G., Teixeira, F.K., Czech, B., Preall, J.B., Zamparini, A.L., Seifert, J.R., Malone, C.D., Hannon, G.J., and Lehmann, R. (2016). Regulation of Ribosome Biogenesis and Protein Synthesis Controls Germline Stem Cell Differentiation. *Cell Stem Cell* *18*, 276–290.
- Schmieder, R., and Edwards, R. (2011). Quality control and preprocessing of metagenomic datasets. *Bioinformatics* *27*, 863–864.
- Schubert, U., Antón, L.C., Gibbs, J., Norbury, C.C., Yewdell, J.W., and Benink, J.R. (2000). Rapid degradation of a large fraction of newly synthesized proteins by proteasomes. *Nature* *404*, 770–774.
- Sherman, M.Y., and Qian, S.B. (2013). Less is more: improving proteostasis by translation slow down. *Trends Biochem. Sci.* *38*, 585–591.
- Signer, R.A., Magee, J.A., Salic, A., and Morrison, S.J. (2014). Haematopoietic stem cells require a highly regulated protein synthesis rate. *Nature* *509*, 49–54.
- Signer, R.A., Qi, L., Zhao, Z., Thompson, D., Sigova, A.A., Fan, Z.P., DeMartino, G.N., Young, R.A., Sonenberg, N., and Morrison, S.J. (2016). The rate of protein synthesis in hematopoietic stem cells is limited partly by 4E-BPs. *Genes Dev.* *30*, 1698–1703.
- Sigurdsson, V., Takei, H., Soboleva, S., Radulovic, V., Galeev, R., Siva, K., Leeb-Lundberg, L.M., Iida, T., Nittono, H., and Miharada, K. (2016). Bile Acids Protect Expanding Hematopoietic Stem Cells from Unfolded Protein Stress in Fetal Liver. *Cell Stem Cell* *18*, 522–532.
- Sontag, E.M., Vonk, W.I.M., and Frydman, J. (2014). Sorting out the trash: the spatial nature of eukaryotic protein quality control. *Curr. Opin. Cell Biol.* *26*, 139–146.
- Taylor, R.C., and Dillin, A. (2011). Aging as an event of proteostasis collapse. *Cold Spring Harb. Perspect. Biol.* *3*, a004440.
- Thompson, B.J., Jankovic, V., Gao, J., Buonamici, S., Vest, A., Lee, J.M., Zavadil, J., Nimer, S.D., and Aifantis, I. (2008). Control of hematopoietic stem cell quiescence by the E3 ubiquitin ligase Fbw7. *J. Exp. Med.* *205*, 1395–1408.
- Trapnell, C., Pachter, L., and Salzberg, S.L. (2009). TopHat: discovering splice junctions with RNA-Seq. *Bioinformatics* *25*, 1105–1111.
- van Galen, P., Kreso, A., Mbong, N., Kent, D.G., Fitzmaurice, T., Chambers, J.E., Xie, S., Laurenti, E., Hermans, K., Eppert, K., et al. (2014). The unfolded protein response governs integrity of the haematopoietic stem-cell pool during stress. *Nature* *510*, 268–272.
- van Galen, P., Mbong, N., Kreso, A., Schoof, E.M., Wagenblast, E., Ng, S.W.K., Krivdova, G., Jin, L., Nakauchi, H., and Dick, J.E. (2018). Integrated Stress Response Activity Marks Stem Cells in Normal Hematopoiesis and Leukemia. *Cell Rep.* *25*, 1109–1117.e5.
- Vilchez, D., Boyer, L., Morante, I., Lutz, M., Merkwirth, C., Joyce, D., Spencer, B., Page, L., Masliah, E., Berggren, W.T., et al. (2012). Increased proteasome activity in human embryonic stem cells is regulated by PSMD11. *Nature* *489*, 304–308.
- Walter, P., and Ron, D. (2011). The unfolded protein response: from stress pathway to homeostatic regulation. *Science* *334*, 1081–1086.
- Wang, F., Durfee, L.A., and Huijbregtse, J.M. (2013). A cotranslational ubiquitination pathway for quality control of misfolded proteins. *Mol. Cell* *50*, 368–378.
- Warr, M.R., Binnewies, M., Flach, J., Reynaud, D., Garg, T., Malhotra, R., Deb-nath, J., and Passequé, E. (2013). FOXO3A directs a protective autophagy program in haematopoietic stem cells. *Nature* *494*, 323–327.
- Wilson, A., Murphy, M.J., Oskarsson, T., Kaloulis, K., Bettess, M.D., Oser, G.M., Pasche, A.C., Knabenhans, C., Macdonald, H.R., and Trumpp, A. (2004). c-Myc controls the balance between hematopoietic stem cell self-renewal and differentiation. *Genes Dev.* *18*, 2747–2763.
- Zismanov, V., Chichkov, V., Colangelo, V., Jamet, S., Wang, S., Syme, A., Koromilas, A.E., and Crist, C. (2016). Phosphorylation of eIF2 α Is a Translational Control Mechanism Regulating Muscle Stem Cell Quiescence and Self-Renewal. *Cell Stem Cell* *18*, 79–90.

STAR★METHODS

KEY RESOURCES TABLE

REAGENT or RESOURCE	SOURCE	IDENTIFIER
Antibodies		
APC Anti-mouse CD3 ϵ (17A2)	BioLegend	Cat #100236
FITC Anti-mouse CD3 ϵ (17A2)	BioLegend	Cat #100204
PE Anti-mouse CD3 ϵ (17A2)	BioLegend	Cat #100206
APC Anti-mouse CD4 (GK1.5)	BioLegend	Cat #100412
FITC Anti-mouse CD4 (GK1.5)	BioLegend	Cat #100406
PE Anti-mouse CD4 (GK1.5)	BioLegend	Cat #100408
APC Anti-mouse CD5 (53-7.3)	BioLegend	Cat #100626
FITC Anti-mouse CD5 (53-7.3)	BioLegend	Cat #100606
PE Anti-mouse CD5 (53-7.3)	BioLegend	Cat #100608
APC Anti-mouse CD8 α (53-6.7)	eBioscience	Cat #17-0081-82
FITC Anti-mouse CD8 α (53-6.7)	eBioscience	Cat #11-0081-85
PE Anti-mouse CD8 α (53-6.7)	eBioscience	Cat #12-0081-83
APC Anti-mouse CD11b (M1/70)	eBioscience	Cat #17-0112-82
APC eFluor780 Anti-mouse CD11b (M1/70)	eBioscience	Cat #47-0112-82
FITC Anti-mouse CD11b (M1/70)	eBioscience	Cat #12-0112-83
PE Anti-mouse CD11b (M1/70)	eBioscience	Cat #11-0112-85
PE/Cy7 Anti-mouse CD16/32 (Fc γ RII/III; 93)	BioLegend	Cat #101318
PerCP/Cy5.5 Anti-mouse CD16/32 (Fc γ RII/III; 93)	BioLegend	Cat #101324
Biotin Anti-mouse CD34 (RAM34)	eBioscience	Cat #13-0341-85
eFluor660 Anti-mouse CD34 (RAM34)	eBioscience	Cat #50-0341-82
Alexa Fluor 700 Anti-mouse CD34 (RAM34)	eBioscience	Cat #56-0341-82
FITC Anti-mouse CD34 (RAM34)	eBioscience	Cat #11-0341-85
FITC Anti-mouse CD43 (R2/60)	eBioscience	Cat #11-0431-85
PE Anti-mouse CD43 (R2/60)	eBioscience	Cat #12-0431-83
APC eFluor 780 Anti-mouse CD45.1 (A20)	eBioscience	Cat #47-0453-82
Alexa Fluor 700 Anti-mouse CD45.2 (104)	BioLegend	Cat #109822
FITC Anti-mouse CD45.2 (104)	BioLegend	Cat #109806
APC Anti-mouse CD45R (B220) (RA3-6B2)	eBioscience	Cat #17-0452-83
FITC Anti-mouse CD45R (B220) (RA3-6B2)	eBioscience	Cat #11-0452-85
PE Anti-mouse CD45R (B220) (RA3-6B2)	eBioscience	Cat #12-0452-85
PerCP-Cyanine5 Anti-mouse CD45R (B220) (RA3-6B2)	eBioscience	Cat #45-0452-82
APC Anti-mouse CD48 (HM48-1)	BioLegend	Cat #103412
FITC Anti-mouse CD48 (HM48-1)	BioLegend	Cat #103404
PE Anti-mouse CD48 (HM48-1)	BioLegend	Cat #103406
PE/Cy7 Anti-mouse CD48 (HM48-1)	BioLegend	Cat #103424
FITC Anti-mouse CD71 (R17217)	eBioscience	Cat #11-0711-85
APC Anti-mouse CD117 (cKit) (2B8)	eBioscience	Cat #17-1171-83
APC eFluor 780 Anti-mouse CD117 (cKit) (2B8)	eBioscience	Cat #47-1711-82
PE-Cyanine7 Anti-mouse CD117 (cKit) (2B8)	eBioscience	Cat #25-1711-82
PE Anti-mouse CD127 (IL7R α ; A7R34)	BioLegend	Cat #135010
APC Anti-mouse CD150 (TC15-12F12.2)	BioLegend	Cat #115910

(Continued on next page)

Continued

REAGENT or RESOURCE	SOURCE	IDENTIFIER
PE Anti-mouse CD150 (TC15-12F12.2)	BioLegend	Cat #115904
PE-Cyanine7 Anti-mouse CD150 (TC15-12F12.2)	BioLegend	Cat #115914
APC Anti-mouse Ter119 (TER-119)	Biolegend	Cat #116212
FITC Anti-mouse Ter119 (TER-119)	Biolegend	Cat #116206
PE Ter119 (TER-119)	Biolegend	Cat #116208
APC Anti-mouse Sca-1 (D7, E13-161.7)	eBioscience	Cat #17-5981-82
Alexa Fluor 700 Anti-mouse Sca-1 (D7, E13-161.7)	eBioscience	Cat #56-5981-82
FITC Anti-mouse Sca-1 (D7, E13-161.7)	eBioscience	Cat #11-5981-85
PerCp-Cyanine5.5 Anti-mouse Sca-1 (D7, E13-161.7)	eBioscience	Cat #45-5981-82
APC Anti-mouse Gr-1 (RB6-8C5)	BioLegend	Cat #108412
FITC Anti-mouse Gr-1 (RB6-8C5)	BioLegend	Cat #108406
PE Anti-mouse Gr-1 (RB6-8C5)	BioLegend	Cat #108408
PE/Cy7 Anti-mouse Gr-1 (RB6-8C5)	BioLegend	Cat #108416
APC Anti-mouse IgM (II/41)	eBioscience	Cat #17-5790-82
PE Anti-mouse IgM (II/41)	eBioscience	Cat #12-5790-83
Streptavidin-PECy7	BioLegend	Cat #405206
Anti-Ubiquitin (P4D1)	Cell Signaling	Cat #3933S
Anti-K48-Polyubiquitin (polyclonal)	Cell Signaling	Cat# 4289S
Anti-c-Myc (polyclonal)	Cell Signaling	Cat# 9402S
Anti-phos-Eif2 α (S51)	Cell Signaling	Cat #9721S
Anti- β -Actin (AC74)	Sigma	Cat #A2228
Anti-Gapdh (14C10)	Cell Signaling	Cat #2118S
HRP-linked anti-rabbit IgG	Cell Signaling	Cat #7074S
HRP-linked anti-mouse IgG	Cell Signaling	Cat #7076S
Chemicals, Peptides, and Recombinant Proteins		
PIPC	GE Healthcare Biosciences Corp	Cat #27473201
Anti-mouse CD117 microbeads	Miltenyi	Cat #130-091-224
TCA	Sigma	Cat #T6399
Triton X-100	CalBiochem	Cat #648466
LDS loading buffer	Life Technologies	Cat #NP007
SDS	Life Technologies	Cat #NP0060
Glycine	Sigma	Cat #50046
Tetraphenylethene maleimide (TMI)	Dr. Yuning Hong	Custom Synthesized
OP-Puro	Medchem Source	Custom Synthesized
SYPRO Ruby Protein Gel Stain	Bio-Rad	Cat #1703125
2-mercaptoethanol	Sigma	Cat #M3148
SYBR green	Roche	Cat #4707516001
Critical Commercial Assays		
SuperSignal West Femto or Pico PLUS chemiluminescence kit	Thermo Scientific	Cat #34095
Click-iT Cell Reaction Buffer Kit	Life Technologies	Cat #C10269
Alexa Fluor 555-conjugated azide	Life Technologies	Cat #A20012
Proteasome-Glo chymotrypsin-like cell based assay	Promega	Cat #G8660
RNeasy Plus Micro Kit	QIAGEN	Cat #74034
RT2 First Strand Kit	QIAGEN	Cat #330404

(Continued on next page)

Continued		
REAGENT or RESOURCE	SOURCE	IDENTIFIER
Deposited Data		
RNA-sequencing data (<i>Aars</i> ^{sti/sti} and <i>Aars</i> ^{+/+} HSCs)	GEO	GSE141008
Experimental Models: Organisms/Strains		
Mouse: B6: C57BL/6J	The Jackson Laboratory	Cat #000664
Mouse: B6SJL: B6.SJL	The Jackson Laboratory	Cat #002014
Mouse: <i>Pten</i> ^{fl/fl}	The Jackson Laboratory	Cat #006440
Mouse: <i>Mx1-Cre</i>	The Jackson Laboratory	Cat #003556
Mouse: <i>Rpl24</i> ^{Bst/+}	The Jackson Laboratory	Cat #000516
Mouse: <i>Aars</i> ^{sti/sti}	The Jackson Laboratory	Cat #002560
Mouse: Ub ^{G76V} -GFP	The Jackson Laboratory	Cat #008111
Mouse: <i>Myc</i> ^{fl}	The Jackson Laboratory	Cat #011123
Oligonucleotides		
<i>Myc</i> forward	IDT	5'- CTTCTCTCCTTCTCCTCGGACTC-3'
<i>Myc</i> reverse	IDT	5'- GGAGATGAGCCCGACTCCGACCTC-3'
β-Actin forward	IDT	5'-CGTCGACAACGGCTCCGGCATG-3'
β-Actin reverse	IDT	5'-GGGCCTCGTCACCCACATAGGAG-3'
Software and Algorithms		
FlowJo	FlowJo, LLC	N/A
FACSDiva	BD Bioscience	N/A
Prism 8	GraphPad	N/A
ImageJ	NIH	N/A
Image Lab 6.0.1	Bio-Rad	N/A
TopHat 1.4.1	JHU CCB	N/A
PRINSEQ Lite 0.20.3	N/A	N/A
Htseq-count 0.7.1	N/A	N/A
Bioconductor package DESeq2 1.6.3	Bioconductor	N/A

LEAD CONTACT AND MATERIALS AVAILABILITY

Further information and requests for resources and reagents should be directed to and will be fulfilled by the Lead Contact, Dr. Robert Signer (rsigner@ucsd.edu). TMI was synthesized by Dr. Yuning Hong and is available from her upon request (Y.Hong@latrobe.edu.au).

EXPERIMENTAL MODEL AND SUBJECT DETAILS

Mice

C57BL/6J, C57BL6.SJL, *Pten*^{fl/fl}, *Mx1-Cre*, *Rpl24*^{Bst/+}, *Aars*^{sti/sti}, Ub^{G76V}-GFP, and *Myc*^{fl} mice were housed in pathogen-free conditions.

Pten^{fl/fl} (Groszer et al., 2006), and *Myc*^{fl} mice (de Alboran et al., 2001) were bred to *Mx1-Cre* (*Cre*⁺) (Kühn et al., 1995) mice to generate *Mx1-Cre*⁺;*Pten*^{fl/fl} and *Mx1-Cre*⁺;*Myc*^{fl} mice, respectively. *Mx1-Cre*⁺;*Pten*^{fl/fl} mice were further crossed to *Rpl24*^{Bst/+} mice (Oliver et al., 2004) to yield *Mx1-Cre*⁺;*Pten*^{fl/fl};*Rpl24*^{Bst/+} mice. *Aars*^{sti/sti} mice (Lee et al., 2006) were bred to *Mx1-Cre*⁺;*Myc*^{fl} mice to produce *Mx1-Cre*⁺;*Myc*^{fl/+};*Aars*^{sti/sti} mice. *Mx1-Cre*⁺;*Pten*^{fl/fl} and *Aars*^{sti/sti} were bred to Ub^{G76V}-GFP mice (Lindsten et al., 2003) to generate *Mx1-Cre*⁺;*Pten*^{fl/fl};*UB*^{G76V}-GFP and *Ub*^{G76V}-GFP;*Aars*^{sti/sti} mice, respectively. Mutant mice were all backcrossed for at least ten generations onto a C57BL background. C57BL6/J (CD45.2) and C57BL6.SJL (CD45.1) mice were used in transplantation experiments.

Both male and female mice between 6 and 12 weeks of age were used in these studies. All mice were housed in the vivarium at the UC San Diego Moores Cancer Center. All protocols were approved by the UC San Diego Institutional Animal Care and Use Committee.

Cell isolation

Bone marrow cells were isolated by flushing the long bones (femurs and tibias) or by crushing the long bones, vertebrae and pelvic bones with a mortar and pestle in Ca^{2+} - and Mg^{2+} -free Hank's buffered salt solution (HBSS; Corning) supplemented with 2% (v/v) heat-inactivated bovine serum (GIBCO). Spleens were prepared by crushing tissues between frosted slides. All cells were filtered through a 40 μm cell strainer to obtain single cell suspensions. Cell number and viability were assessed with a hemocytometer based on trypan blue exclusion.

METHOD DETAILS

PIPC treatment

Expression of *Mx1-Cre* was induced by three or four intraperitoneal injections of 10 mg polyinosinic-polycytidylic acid (pIpC; GE Healthcare) administered every other day, beginning at approximately 6 weeks of age.

Proteasome inhibition

For proteasome inhibition experiments, mice were administered bortezomib (Cell Signaling; 1 mg/kg) diluted in 10% (v/v) DMSO via retro-orbital injection.

Flow cytometry and sorting

For flow cytometric analysis and isolation of specific hematopoietic progenitors, cells were incubated with combinations of antibodies to the following cell-surface markers, conjugated to FITC, PE, PerCP-Cy5.5, APC, PE-Cy7, eFluor 660, Alexa Fluor 700, APC-eFluor 780 or biotin (antibody clones are given in brackets in the following list): CD3 ϵ (17A2), CD4 (GK1.5), CD5 (53-7.3), CD8 α (53-6.7), CD11b (M1/70), CD16/32 (Fc γ R1II/III; 93), CD34 (RAM34), CD43 (R2/60), CD45.1 (A20), CD45.2 (104), CD45R (B220; RA3-6B2), CD48 (HM48-1), CD71 (R17217), CD117 (cKit; 2B8), CD127 (IL7R α ; A7R34), CD150 (TC15-12F12.2), Ter119 (TER-119), Sca-1 (D7, E13-161.7), Gr-1 (RB6-8C5) and IgM (II/41). For isolation of HSCs and MPPs, Lineage markers included CD3, CD5, CD8, B220, Gr-1 and Ter119. For isolation of CMPs, GMPs and MEPs, these Lineage markers were supplemented with additional antibodies against CD4 and CD11b. Biotinylated antibodies were visualized by incubation with PE-Cy7 conjugated streptavidin. All reagents were acquired from eBiosciences, or BioLegend. All incubations were for 30-90 min on ice.

HSCs, MPPs, CD34⁺CD16/32^{low}CD127⁻Lineage⁻Sca-1⁻c-kit⁺ CMPs (Akashi et al., 2000), CD34⁺CD16/32^{high}CD127⁻Lineage⁻Sca-1⁻c-kit⁺ GMPs (Akashi et al., 2000), and CD34⁺CD16/32^{-low}CD127⁻Lineage⁻Sca-1⁻c-kit⁺ MEPs (Akashi et al., 2000) were pre-enriched by selecting c-kit⁺ cells using paramagnetic microbeads and an autoMACS magnetic separator (Miltenyi Biotec) before sorting.

Non-viable cells were excluded from sorts and analyses using 4',6-diamidino-2-phenylindole (DAPI). Apoptotic cells were identified using APC annexin V (BDBiosciences). Proliferation was assessed by administering 5-bromo-2'-deoxyuridine (BrdU; Sigma) to mice. BrdU dissolved in PBS was administered with an initial intraperitoneal injection (2 mg) and then mice were maintained on drinking water containing 1 mg/ml BrdU for 72 h. BrdU incorporation in HSCs was measured using the APC BrdU Flow Kit (BD Biosciences).

For analysis of ubiquitylated protein following cell surface staining, cells were fixed in 0.5 mL of 1% paraformaldehyde (Affymetrix) in PBS for 10-15 min on ice. Cells were washed in PBS, then permeabilized in 200 mL PBS supplemented with 3% (v/v) fetal bovine serum (Life Technologies) and 0.1% (m/v) saponin (Sigma) for 5 min at room temperature (20–25°C). Cells were then incubated with anti-ubiquitylated protein antibody (clone FK2, Millipore) at a concentration of 1:500 for 30 min at room temperature. This was followed by incubation with anti-mouse Alexa Fluor 488 (Thermo Scientific) at a concentration of 1:500 for 30 min at room temperature. Cells were washed twice in PBS supplemented with 3% fetal bovine serum and 0.1% saponin, then resuspended in PBS supplemented with DAPI (4 mg/ml final concentration) and analyzed by flow cytometry.

Data acquisition and cell sorting were performed on a FACSAria II, LSR II or FACSCanto flow cytometer (BD Biosciences). Sorted fractions were typically double sorted to ensure high purity. Data were analyzed by FlowJo (TreeStar) software.

Competitive repopulation assay

Adult recipient mice (CD45.1) were administered a minimum lethal dose of radiation using a Mark I Cesium source irradiator (J.L. Sheperd) to deliver two doses of 550 rad (1,100 rad in total) at least 4 h apart. Cells were injected into the retro-orbital venous sinus of anaesthetized recipients. For competitive bone marrow transplants 5×10^5 donor and 5×10^5 recipient-type cells were transplanted. For HSC transplants 10 donor CD150⁺CD48⁻Lineage⁻Sca-1⁺c-kit⁺ HSCs and 2×10^5 recipient-type bone marrow cells were transplanted. Blood was obtained from the tail veins of recipient mice every 4 weeks for at least 16 weeks after transplantation. Red blood cells were lysed with ammonium chloride potassium buffer. The remaining cells were stained with antibodies against CD45.2, CD45.1, CD45R (B220), CD11b, CD3 and Gr-1 to assess donor-cell engraftment.

For secondary transplants, 3×10^6 bone marrow cells collected from primary recipients were transplanted non-competitively into irradiated recipient mice. Primary recipients used for secondary transplantation had long-term multilineage reconstitution by donor cells and median levels of donor-cell reconstitution for the treatments from which they originated. Mice that died over the course of transplantation experiments were omitted from the analyses.

For MPP transplants, 50 CD150⁺CD48⁻Lineage⁻Sca-1⁺c-kit⁺ MPPs and 2x10⁵ recipient-type bone marrow cells were transplanted. Blood was obtained from the tail veins of recipient mice 3,5 and 7 weeks after transplantation.

Western blot analysis

Equal numbers of cells from each stem or progenitor population were sorted into trichloroacetic acid (TCA, Sigma). The final concentration was adjusted to 10% (v/v) TCA. Extracts were incubated on ice for at least 15 min and centrifuged at 15,000 g at 4°C for 15 min. Precipitates were washed in acetone twice and dried. The pellets were solubilized in 9 M urea, 2% (v/v) Triton X-100, and 1% DTT. LDS loading buffer (Life Technologies) was added and the pellet was heated at 70°C for 10 min. Samples were separated on Bis-Tris polyacrylamide gels (Life Technologies) and transferred to PVDF membranes (Bio-Rad). Western blot analyses were performed according to the protocol from Cell Signaling Technologies. Blots were stripped with 1% SDS, 25 mM glycine (pH 2) before re-probing. The following primary and secondary antibodies were used for western blot analyses: Ubiquitin (P4D1; Cell Signaling), K48-Ubiquitin (polyclonal; Cell Signaling 4289), c-Myc (polyclonal; Cell Signaling 9402S), phospho-Eif2 α (S51; Cell Signaling) β -Actin (AC74; Sigma), Gapdh (14C10; Cell Signaling), HRP-linked anti-rabbit IgG (Cell Signaling) and HRP-linked anti-mouse IgG (Cell Signaling). Blots were developed with the SuperSignal West Femto or Pico PLUS chemiluminescence kit (Thermo Scientific).

Measurement of unfolded proteins

4x10⁶ bone marrow cells were stained for cell surface markers as described above. After staining, cells were washed twice in Ca²⁺- and Mg²⁺-free PBS. Tetraphenylethene maleimide (TMI; stock 2 mM in DMSO) was diluted in PBS (50 μ M final concentration), added to each sample and samples were incubated at 37°C for 45 minutes. Samples were washed twice in PBS and analyzed by flow cytometry. DAPI was omitted from these samples because of spectral overlap.

To assess the effects of heat shock, 10⁶ BM cells were incubated Ca²⁺- and Mg²⁺-free HBSS (Corning) supplemented with 2% heat-inactivated bovine serum at 37°C or 42°C for 4 h. Cells were then washed twice in Ca²⁺- and Mg²⁺-free PBS (Corning), and TMI was added as described above.

In vivo measurement of protein synthesis

OP-Puro (Medchem Source; 50 mgkg⁻¹ body mass; pH 6.4–6.6 in PBS) was injected intraperitoneally. One hour later mice were euthanized. Bone marrow was collected, and 4x10⁶ cells were stained with combinations of antibodies against cell-surface markers as described above. After washing, cells were fixed in 0.5 mL of 1% paraformaldehyde (Affymetrix) in PBS for 10–15 min on ice. Cells were washed in PBS, then permeabilized in 200 mL PBS supplemented with 3% (v/v) fetal bovine serum (Life Technologies) and 0.1% (m/v) saponin (Sigma) for 5 min at room temperature (20–25°C). The azide-alkyne cycloaddition was performed using the Click-iT Cell Reaction Buffer Kit (Life Technologies) and azide conjugated to Alexa Fluor 555 (Life Technologies) at 5 mM final concentration. After the 30-min reaction, the cells were washed twice in PBS supplemented with 3% fetal bovine serum and 0.1% saponin, then resuspended in PBS supplemented with DAPI (4 mgml⁻¹ final concentration) and analyzed by flow cytometry (Hidalgo San Jose and Signer, 2019).

In vitro analysis

Colony forming units were assessed by sorting 500 live bone marrow cells per well of a 96-well plate (24 wells per mouse) containing methylcellulose culture medium (M3434; STEMCELL Technologies). Colonies were counted after 14 days.

Cell volume

Average diameter was measured by sorting cells into flat-bottom 96-well plates and analyzing micrographs with ImageJ software. Cell volume was calculated based on the assumption that cells are spherical ($4/3\pi r^3$).

Protein content

Equal numbers of cells from each stem or progenitor population were sorted into HBSS supplemented with 2% (v/v) heat-inactivated bovine serum (GIBCO). Samples were washed once with PBS and centrifuged at 2500 g at 4°C for 5 min. Supernatant was discarded and protein pellets were directly lysed and solubilized in 9M urea, 2% SDS, 50 mM DTT, and 50 mM Tris pH 7.4. After incubating the samples for 10–15 min at room temperature, LDS loading buffer (Life Technologies) was added and the sample was heated at 70°C for 10 minutes. Samples were separated on Bis-Tris polyacrylamide gels (Life Technologies). The Bis-Tris polyacrylamide gels were then stained with SYPRO Ruby Protein Gel Stain (Bio-Rad) for 3 h and washed in a solution containing 7% acetic acid and 10% methanol for 1 h. Gels were imaged using Gel Doc XR (Bio-Rad) and analyzed with Image Lab 6.0.1 software (Bio-Rad).

For bone marrow cells, incubated at 37°C or 42°C, 10⁵ cells were sorted into TCA. The final concentration was adjusted to 10% TCA. Extracts were incubated on ice for at least 15 min and centrifuged at 15,000 g at 4°C for 15 min. Precipitates were washed in acetone twice and dried. The pellets were solubilized in 6 M urea, 2% (v/v) Triton X-100, and 1% (v/v) 2-mercaptoethanol. The protein content in the supernatant was assessed with the microBCA assay (Pierce).

Proteasome activity

5x10³ cells from each cell population were plated into 96-well plates in triplicate. Proteasome activity was measured with the Proteasome-Glo chymotrypsin-like cell based assay (Promega). Luminescence was monitored after a 15 min incubation using a Synergy HTX multi-mode plate reader. HSCs/MPPs incubated with 100 μM MG132 were used as controls.

RNA sequencing

For RNA-seq analysis, total RNA was extracted from ~3000 HSCs using the RNeasy Plus Micro Kit (QIAGEN). Illumina mRNA libraries were prepared using the SMARTseq2 protocol (Picelli et al., 2014). 2.6 μL of total RNA was used in the SMARTSeq2 protocol (70pg to 1.62ng). 18 cycles of PCR were performed for the cDNA preamplification step and 12 cycles were performed for the tagmentation library preparation. The resulting libraries were pooled and deep sequenced in two lanes on the Illumina HiSeq 2500 in high output mode using single-end reads with lengths of 50 nucleotides (25–35M reads per condition). The single-end reads that passed Illumina filters were filtered for reads aligning to tRNA, rRNA, adaptor sequences, and spike-in controls. The reads were then aligned to the mm10 reference genome using TopHat (v 1.4.1) (Trapnell et al., 2009). DUST scores were calculated with PRINSEQ Lite (v 0.20.3) (Schmieder and Edwards, 2011) and low-complexity reads (DUST > 4) were removed from the BAM files. The alignment results were parsed via the SAMtools (Li et al., 2009) to generate SAM files. Read counts to each genomic feature were obtained with the htseq-count program (v 0.7.1) (Anders et al., 2015) using the “union” option. After removing absent features (zero counts in all samples), the raw counts were then imported to Bioconductor package DESeq2 (v 1.6.3) (Love et al., 2014) to identify differentially expressed genes among samples. P values for differential expression are calculated using the Wald test for differences between the base means of two conditions. These P values are then adjusted for multiple test correction using Benjamini Hochberg algorithm. We considered genes differentially expressed between two groups of samples when the DESeq2 analysis resulted in an adjusted P value of < 0.10 and the difference in gene expression was at least 2-fold. Principal Component Analysis (PCA) was performed using the ‘prcomp’ function in R. Heatmaps of differentially expressed genes were generated from log₂(RPKM+1) values using the function heatmap.2(package gplots) in R. GSEA with classic scoring scheme was run for the geneset Biological processes (c5.bp.v6.1.symbols.gmt) from MSigDB on pre-ranked gene lists. For genes with log₂FoldChange greater than zero, a rank -log₁₀(pValue) was assigned and for genes with log₂FoldChange less than zero, a rank of log₁₀(pValue) was assigned.

Quantitative PCR

Cells were sorted directly into RLT plus buffer (QIAGEN) supplemented with 2-mercaptoethanol. RNA was extracted with the RNeasy micro plus kit (QIAGEN) and cDNA was synthesized with the RT2 First Strand Kit (QIAGEN). Reactions were run in 20 μL volumes with SYBR green and a LightCycler 480 (Roche Applied Science). Primer sequences were: *Myc* F, 5'- CTTCTCTCCTTCCTCGGACTC-3'; *Myc* R 5'- GGAGATGAGCCCGACTCCGACCTC-3'; β-Actin F, 5'-CGTCGACAACGGCTCCGGCATG-3'; β-Actin R, 5'-GGGCC TCGTCACCCACATAGGAG-3'

QUANTIFICATION AND STATISTICAL ANALYSIS

Group data are represented by mean ± standard deviation, except for transplantation data which are represented as mean ± standard error of the mean. To test statistical significance between two samples, two-tailed Student's t tests were used. When multiple samples were compared, statistical significance was assessed using a one-way ANOVA or a repeated-measures one-way ANOVA (when comparing multiple time points or populations from the same mouse) followed by Dunnett's test for multiple comparisons. Statistical significance comparing overall numbers of mice with long-term multilineage reconstitution was assessed by a Fisher's exact test. Statistical tests were performed using GraphPad Prism software. The specific type of test used for each figure panel is described in the figure legends, except for the RNA sequencing data which is described in the “RNA sequencing” paragraph of the STAR Methods section above.

For normalized data, means were calculated and statistical tests were performed using log₁₀-transformed data and then means were back-transformed to prevent data skewing. No randomization or blinding was used in any experiments. The only mice excluded from any experiment were those that died after transplantation.

DATA AND CODE AVAILABILITY

The RNA-sequencing data comparing *Aars*^{sti/sti} and control HSCs is available at Gene Expression Omnibus: GSE141008.

Cell Reports, Volume 30

Supplemental Information

Modest Declines in Proteome Quality

Impair Hematopoietic Stem Cell Self-Renewal

Lorena Hidalgo San Jose, Mary Jean Sunshine, Christopher H. Dillingham, Bernadette A. Chua, Miriama Kruta, Yuning Hong, Danny M. Hatters, and Robert A.J. Signer

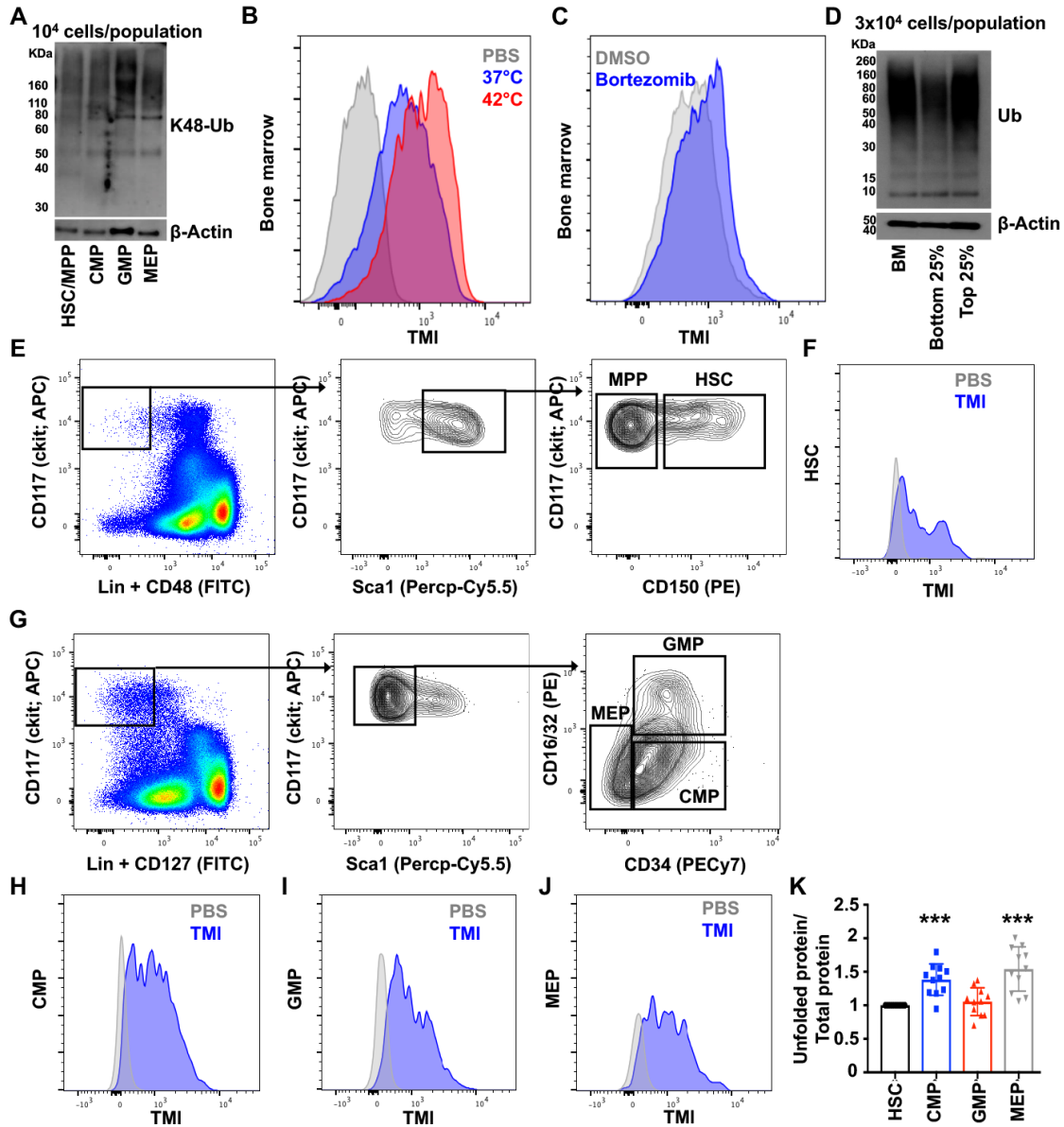


Figure S1. Quantifying unfolded protein abundance within hematopoietic stem and progenitor cells with TMI. Related to Figure 1.

(A) Western blot examining LysK48-ubiquitylated protein in 10^4 HSCs/MPPs, CMPs, GMPs and MEPs (one of two representative blots). (B) Representative histogram showing TMI fluorescence in bone marrow cells after a 4 h incubation at 37°C or 42°C. (C) Representative histogram showing TMI fluorescence in bone marrow cells from mice treated 18 h earlier with bortezomib (BZ) or vehicle (DMSO). (D) Western blot analysis showing ubiquitylated protein in 3×10^4 unfractionated bone marrow cells, as well as bone marrow cells with low (lowest quartile, bottom 25%) and high (highest quartile, top 25%) of TMI fluorescence. (E) Representative flow cytometry plots showing gating strategies for analysis and isolation of HSCs and MPPs. (F) Representative histograms showing TMI fluorescence in HSCs. The background from PBS treated controls is shown in gray. (G) Representative flow cytometry plots showing gating strategies for analysis and isolation of CMPs, GMPs and MEPs. (H-J) Representative histograms showing TMI fluorescence in CMPs (H), GMPs (I) and MEPs (J). The background from PBS treated controls is shown in gray. (K) TMI fluorescence relative to total protein content in HSCs, CMPs, GMPs and MEPs (data from Fig. 1F,L). Data in K represent mean \pm standard deviation. Statistical significance was assessed using an ANOVA followed by Dunnett's multiple comparisons test relative to HSCs. *** $P < 0.001$.

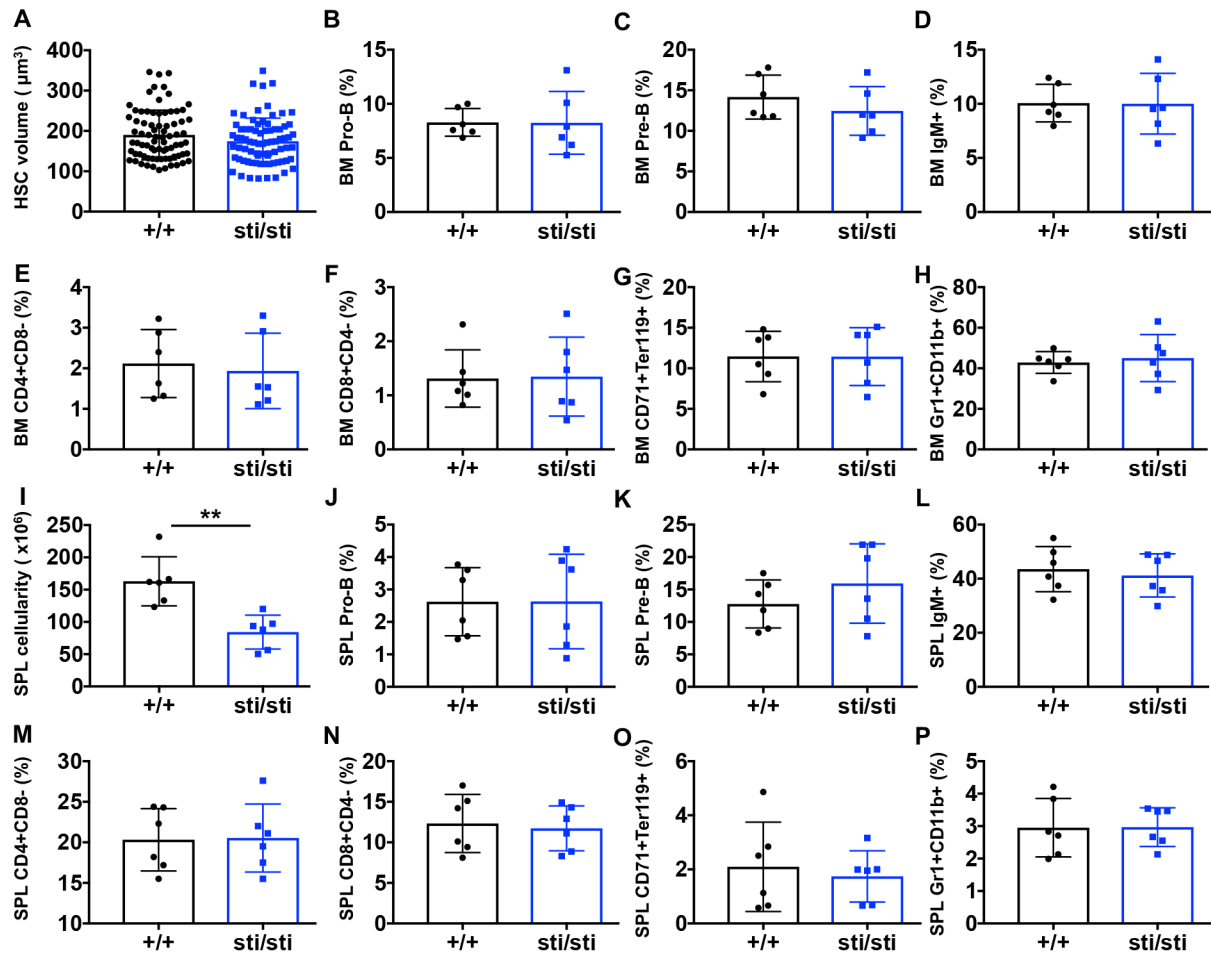


Figure S2. *Aars*^{sti/sti} mice have normal frequencies of lymphoid, myeloid and erythroid lineage cells. Related to Figure 2.

(A) Cell volume of wild-type (+/+) and *Aars*^{sti/sti} (sti/sti) HSCs (n ≥ 78 cells/population). (B-P) Frequency of IgM⁻ CD45R(B220)⁺CD43⁺ pro-B cells (Hardy et al., 1991), IgM⁻CD45R(B220)⁺CD43⁻ pre-B cells (Hardy et al., 1991), IgM⁺CD45R(B220)⁺ B cells (D, L), CD4⁺CD8⁺ T cells (E, M) CD4⁻CD8⁺ T cells, (F, N) CD71⁺Ter119⁺ erythroid cells (Zhang et al., 2003) and CD11b⁺Gr1⁺ myeloid cells (H, P) in the bone marrow (B-H) and spleen (J-P) of wild-type (+/+) and *Aars*^{sti/sti} mice (n = 6 mice per genotype). (I) Spleen (SPL) cellularity in wild-type (+/+) and *Aars*^{sti/sti} (sti/sti) mice (n = 6 mice per genotype). Data represent mean ± standard deviation. Statistical significance was assessed using a two-tailed Student's t-test. **P<0.01.

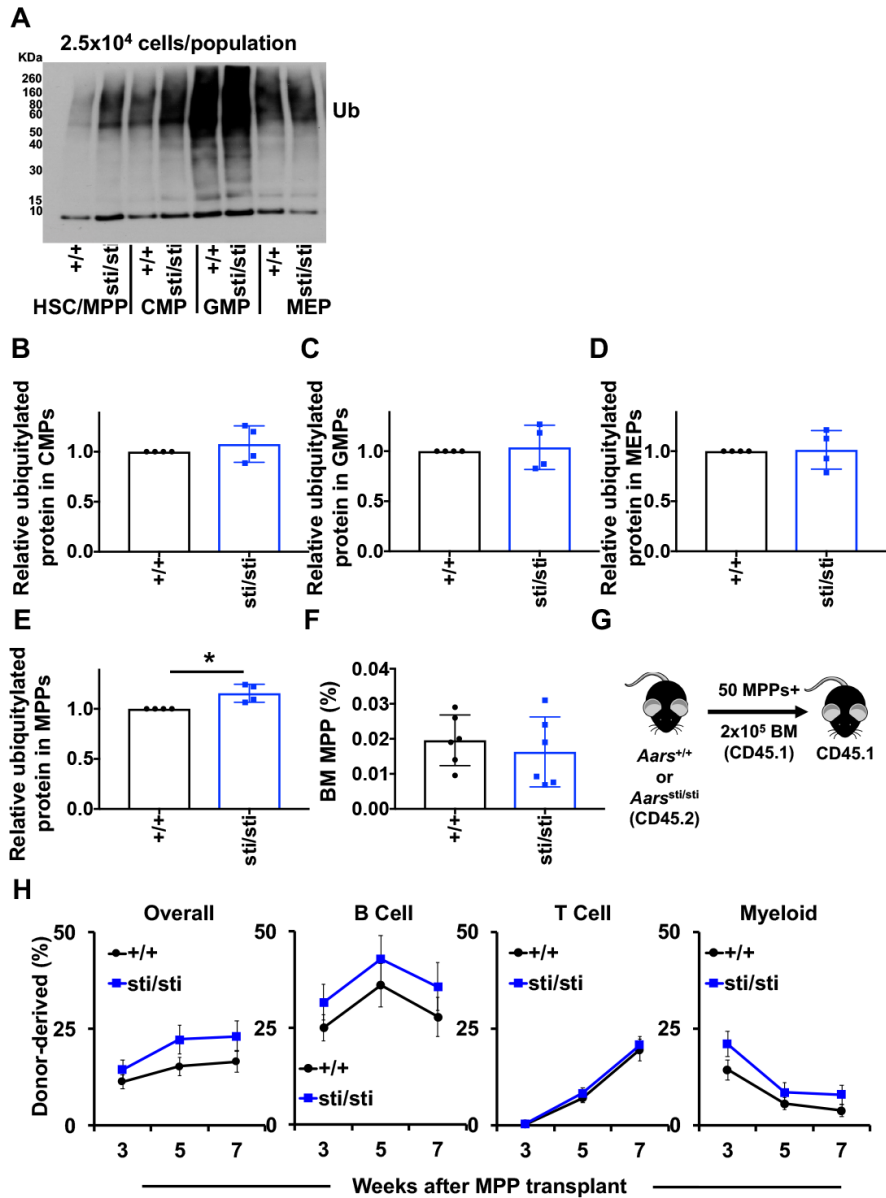


Figure S3. *Aars*^{sti/sti} MPPs have normal capacity to reconstitute irradiated mice in short-term transplantation. Related to Figure 2. (A-D) Flow cytometry analysis showing relative ubiquitylated protein content in *Aars*^{sti/sti} (*sti/sti*) relative to wild-type (*+/+*) CMPs (A), GMPs (B), MEPs (C) and MPPs (D) (*n* = 4 mice per genotype). (E) Frequency of MPPs in the bone marrow of wild-type (*+/+*) and *Aars*^{sti/sti} mice (*n* = 6 mice per genotype). (F) Diagram showing MPP transplantation strategy. (G) Donor cell engraftment when 50 CD150⁺CD48⁺LSK MPPs from wild-type (*+/+*) and *Aars*^{sti/sti} (*sti/sti*) mice were transplanted along with 2x10⁵ recipient bone marrow cells into irradiated mice (*n* = 3 donors and 15 recipients per genotype). Data represent mean ± standard deviation (A-E) or standard error of the mean (G). Statistical significance was assessed using a two-tailed Student's *t*-test. **P*<0.05.

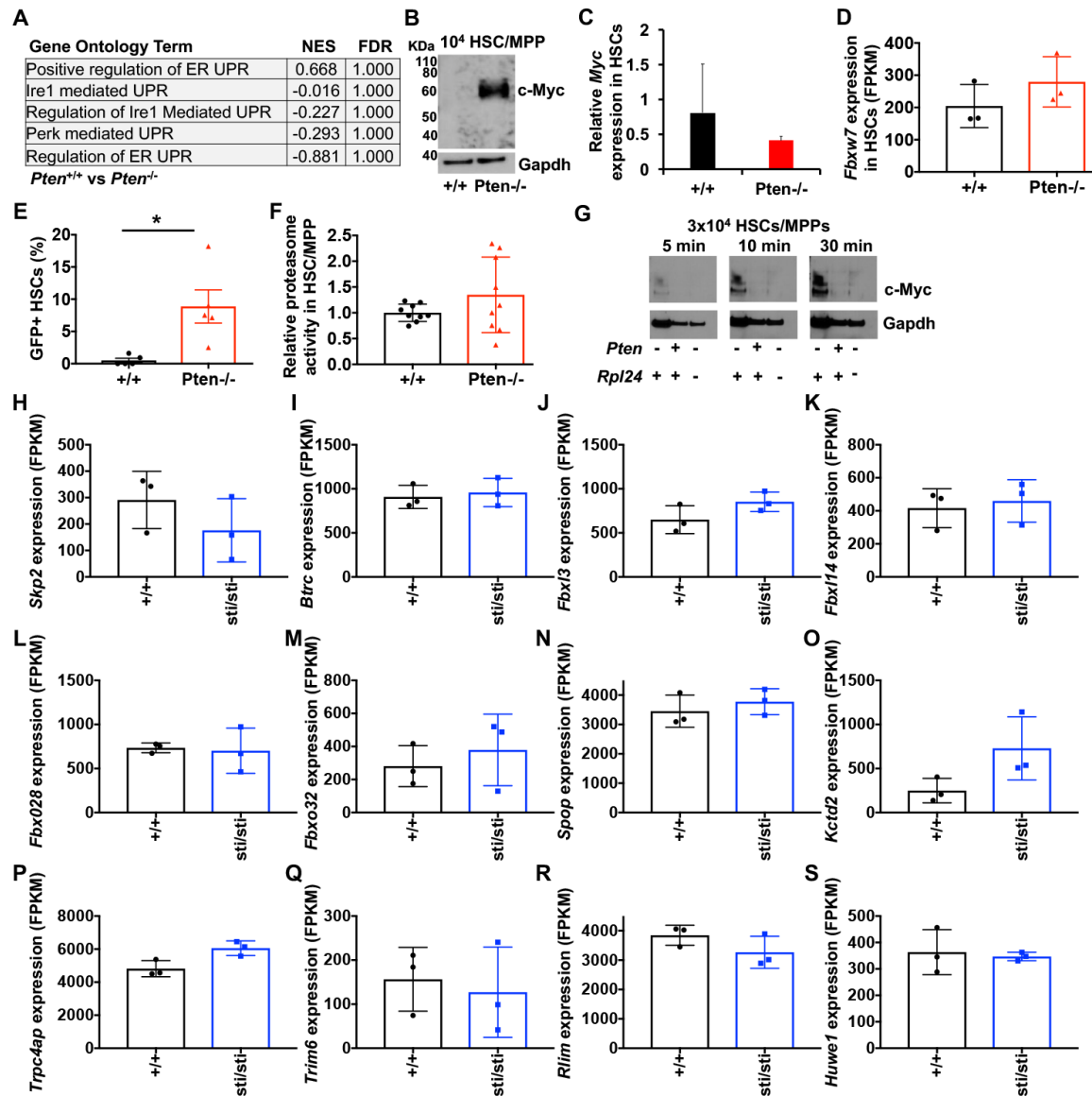


Figure S4. Accumulation of ubiquitylated protein overwhelms the proteasome leading to c-Myc stabilization in HSCs. Related to Figure 3.

(A) Gene set enrichment analysis demonstrating no significant activation of the UPR^{ER} in *Pten^{fl/fl}* (*Pten^{+/+}*) as compared to *Mx1-Cre⁺;Pten^{fl/fl}* (*Pten^{-/-}*) HSCs. (B) Western blot examining c-Myc protein in 10⁴ HSCs/MPPs isolated from *Pten^{fl/fl}* (*+/+*) and *Mx1-Cre⁺;Pten^{fl/fl}* (*Pten^{-/-}*) mice (one of three representative blots). (C) *Myc* mRNA expression normalized to β -Actin in *Pten^{fl/fl}* (*+/+*) and *Mx1-Cre⁺;Pten^{fl/fl}* (*Pten^{-/-}*) HSCs (n = 3 per genotype). (D) *Fbxw7* expression in *Pten^{fl/fl}* (*+/+*) and *Mx1-Cre⁺;Pten^{fl/fl}* (*Pten^{-/-}*) HSCs (n = 3 per genotype). (E) Frequency of HSCs that are GFP⁺ in the bone marrow of Ub^{G76V}-GFP (*+/+*) and *Mx1-Cre⁺;Ub^{G76V}-GFP;Pten^{fl/fl}* (*Pten^{-/-}*) mice (n = 4-5 mice per genotype). (F) Relative proteasome activity in *Pten^{fl/fl}* (*+/+*) and *Mx1-Cre⁺;Pten^{fl/fl}* (*Pten^{-/-}*) HSCs HSCs/MPPs (n = 9 replicates per genotype in 3 experiments). (G) Western blot examining ubiquitylated protein in 3x10⁴ wild-type (*Pten^{fl/fl};Rpl24^{+/+}*), *Pten*-deficient mice (*Mx1-Cre⁺Pten^{fl/fl};Rpl24^{+/+}*) and in *Mx1-Cre⁺;Pten^{fl/fl};Rpl24^{Bst/+}* HSCs/MPPs. Exposure times of 5, 10 and 30 minutes are shown. (H-S) Expression of E3 ubiquitin ligases that target c-Myc is not reduced in *Aars^{sti/sti}* HSCs. Expression of (H) *Skp2*, (I) *Btrc*, (J) *Fbxl3*, (K) *Fbxl14*, (L) *Fbxo28*, (M) *Fbxo32*, (N) *Spop*, (O) *Kctd2*, (P) *Trpc4ap*, (Q) *Trim6*, (R) *Rlim* and (S) *Huwe1* in wild-type (*+/+*) and *Aars^{sti/sti}* (*sti/sti*) HSCs based on RNA sequencing (n = 3 per genotype). Data represent mean \pm standard deviation. Statistical significance was assessed using a Student's t-test (C-F; *P<0.05). Adjusted P values (H-S) did not reach the threshold of statistical significance for any of these genes.